Drying of Supported Catalysts: A Reduced Parameter Model for High Concentration Nickel-Alumina Systems

By

ANUSHA VALLAL NOORITHAYA

A thesis submitted to the

School of Graduate Studies

Rutgers, The State University of New Jersey

In partial fulfillment of the requirements

For the degree of

Master of Science

Graduate Program in Chemical and Biochemical Engineering

Written under the direction of

Benjamin J. Glasser

And approved by

_____

_____

_____

New Brunswick, New Jersey

May 2018

ABSTRACT OF THE THESIS

Drying of Supported Catalysts: A Reduced Parameter Model for High Concentration Nickel-Alumina Systems

By ANUSHA VALLAL NOORITHAYA

Thesis Director:

Dr. Benjamin J. Glasser

Supported catalysts are widely used in many industries. Manufacturing these catalysts is extremely complex and these processes are influenced by many interdependent parameters. Although their performance and activity are the most critical properties, their structures and design are also critical to their effectiveness. Research work showed how the adsorption of metal on the catalyst support and film breakage could significantly influence metal distributions at lower concentrations. A nickel nitrate hexahydrate-alumina system was studied. It was observed that at higher concentrations, the adsorption parameters were no longer the controlling factor, and solution properties began to take over the metal distribution characteristics. Solution properties like density, viscosity, surface tension and volume ratio of metal begin to take over the metal distribution at these high concentrations. At very high concentrations (about 3.0 M), a uniform metal distribution profile was observed due to the high concentration and low melting point of the metal salt, leading to a molten liquid phase during drying. This model which was based on nickel nitrate hexahydrate, exhibited a good agreement with experimental

results. To apply this model to other metal-support systems, a lot of experiments would have to be repeated to determine the metal solution properties as they are unique to different metal-support combinations. In this thesis, we designed and created a simplified model based on the high-concentration nickel nitrate hexahydrate model. This model can be applied to other metals on an Alumina support and can simulate their metal distributions after the drying process. Designing this model involved a detailed analysis of each of the solution based parameters and adsorption parameters considered for nickel nitrate. A reduced parameter model involving fewer parameters was developed and tested using a new metal precursor - cobalt nitrate hexahydrate. Experiments were then performed for cobalt nitrate hexahydrate on alumina supports and their parameters were incorporated into the model. Post drying metal distributions for different concentrations of the metal solutions were generated using this model.

Acknowledgement

I would consider myself to be tremendously fortunate to have Dr. Benjamin J. Glasser as my advisor, without whom, this would have been an impossible task. I would like to express my sincere gratitude to him for his patient guidance throughout my thesis both professionally and personally.

I would also like to thank my colleague and student mentor, Cody Bishop, who has been very patient and an excellent teacher. His valuable knowledge and experience made this an easy journey. I would like to take this opportunity to express my appreciation towards all the memebers of the Rutgers Catalyst Manufacturing Consortium for their valuable ideas and feedback. I would also like to thank Dr. Xue Liu for his valueable contribution towards my thesis. As a part of Dr. Glasser's research group, I got to work with some amazing colleagues: Hao, Yangyang, Veerakiet, Pavithra, Chaitanya, Prateek, Sahil and many more. I would like to thank them for their support and encouragement.

I would like to thank Dr. Georgios Tsilomelekis and Dr. Haoran Zhang for accepting the invitation to be on my thesis committee and also for their constructive feedback and comments.

I cannot express how grateful I am towards my parents and family. The sacrifices they made and the unconditional love they showed is the reason I am here today. I would also like to thank my friends who have been creating wonderful memories throughout my life.

Table of Contents

List of Figures:

1. Introduction

Catalysts play an essential role in several industries like petrochemicals, oil and gas, pharmaceuticals and food processing. They are manufactured in various forms and types (like homogenous, heterogeneous, extrudates, powders, organics, precious metals etc.) which are tailored to suit their use in industries. Although catalysis and reaction kinetics are important to conduct and control the chemical reactions, the structure and design of a catalyst can have significant effects on reaction productivity. An ideal catalyst has high activity, selectivity and stability. [1]

In supported catalysts, the active phase of a catalyst can be deposited on a variety of supports which are highly porous. They can vary from small powders to centimeter-sized pellets. [2] Among the various transition alumina materials, γ-alumina is widely used as a catalyst support in industries. This is because of its desired textural properties such as surface area, pore size distribution and pore-volume. Its acidic/basic characteristics are mainly due to surface chemical composition, local micro structure, and phase composition. [3] Apart from alumina, other commonly used supports are silica, carbon and clay supports. [4]

Preparation of catalyst supports often involve a combination of 3-4 different unit operations which can be described as: (i) introduction of the metal precursor on the support by impregnation, ion-exchange, co-precipitation and deposition precipitation, (ii) drying of catalyst, and (iii) calcination [1]

Different metal distribution profiles like uniform, egg-shell, egg-yolk and egg white are obtained by aforementioned steps. These different distributions of metals are useful for different types of reactions. For example, egg-shell catalysts would give higher activity in instantaneous reactions whereas egg white catalysts would perform better with abrasive environments and slow reactions. [5]

Impregnation of the metal precursor through the volume of the support can be done in different ways. This could also strongly affect the final metal profiles. Commonly used impregnation methods are dry impregnation, wet impregnation, strong electrostatic adsorption, deposition-precipitation, ion exchange, and reactive adsorption. [1] In the dry impregnation method, a quantity of metal solution equal to the pore volume of the support, is used for impregnation. This method doesn't require filtration and the metal content is known. However, there could be a limited metal interaction with the support. This method is commonly used in industries for impregnating precious metals like palladium. Contrary to dry impregnation, the wet impregnation method uses a solution of metal precursor in excess to the pore volume of support. Here, the mixing is improved and weaker adsorbing metals are filtered away. On the other hand, metal loadings must be measured and the solution should be filtered. This method is generally applied to cheaper base metal precursors like nickel and copper, where having excess precursor is not too expensive. [1]

After impregnation, the supports are generally dried at temperatures between 80^0C and 200^0C to remove the solvent used during impregnation. [6] The drying process in a chemical process industry can be defined as the vaporization and removal of water or other liquids from a solution, suspension, or any other mixtures, to form a dry solid. It is a complex process that involves simultaneous heat and mass transfer, accompanied by physicochemical transformations. Depending on the mechanism of heat transfer, drying can be broadly categorized into direct heating (convection), indirect or contact (conduction), radiant (radiation) and dielectric or microwave (radio frequency) drying. [7]

The critical aspects of a drying process are heat and mass transfer. Heat is transferred to the product to evaporate liquid, and mass is transferred as a vapor into the surrounding gas. The drying rate is determined by a set of factors that affect heat and mass transfer. Solids drying is generally understood to follow two distinct drying zones, the constant-rate period and the falling-rate period. The two zones are distinguished by a break point called the critical moisture content. During the constant-rate period, moisture vaporizes into the air stream and the controlling factor is the transfer coefficient for diffusion across the gas film. The moisture movement during the falling period is important and hence two models i.e., the diffusion theory and the capillary theory are used to describe the physical nature of this process. In the diffusion theory, the rate of water movement to the air interface is governed by rate equations similar to those for heat transfer. Whereas, in

the capillary theory the forces controlling the movement of water are capillary in origin, arising from the minute pore spaces between the individual particles. Apart from a heat driven drying process, one could also dry using vacuum drying and freeze-drying techniques. During freeze-drying, the water is frozen, and liquid flow under capillary action is impossible and hence the movement of moisture is by vapor diffusion. [8]

The endpoint of drying is also an equally important part of a drying process. There are several approaches to determine the endpoint of the drying process. A common method is to construct a drying curve by taking samples during different stages of a drying cycle against the drying time. When the drying is complete, a rise in the product temperature is observed, indicating the completion of drying at a specific, desired moisture content. [7]

Drying equipment are generally classified on the basis of various factors like the drying temperature, pressure, method of heating, heating medium, air circulation, feeding etc. A variety of dryers are used in the chemical industry, such as tunnel dryers, tray dryers, rotary dryers, drum dryers, etc. [8] After drying, catalysts are often calcined to decompose them or to drive away volatile matter, at temperatures above 500^0C and many a times calcination affects the activity of the final catalyst. [9]

The drying process is also known to affect the activity and performance of a catalyst. Large variations are sometimes observed between the metal distribution results obtained after impregnation and after drying. Some factors that significantly influence the metal redistribution are the rate of heating,

degree of liquid saturation, liquid viscosity, pore volume, and pore size distribution. [1] A lot of experimental work has been carried out on investigating the effect of drying on metal redistribution. [10, 11] It was observed that drying could have significant effects on the metal distribution in the case of weak or moderate adsorption of metal on the support, although its effect is not significant for strong adsorption. It was also seen how the initial metal concentrations affected the metal distributions after drying, provided we begin from a uniform initial condition. [5, 12] In the case of weak absorbing metals drying at a higher rate leads to an increase in concentration at the external surface and in the case of lower drying rates there is more uniform distribution. It was also observed that the drying rate could affect the surface accumulation of metal with copper-alumina catalysts. [13] Neimark et al [14] were amongst the early researchers to theoretically study a drying process, wherein they used a dimensionless number to characterize the drying regimes. Komiyama et al [10] proposed a “reservoir” model to represent drying, wherein a porous structure is described as a support with a small number of macro-pores and large number of micro-pores. [15] Due to capillary pressure, the liquid solution is drawn from the macro-pores to the micro-pores, which works as a “reservoir”. Lee et al [11] studied the redistribution of metal during drying using a model with a capillary tube. Here evaporation takes place at one end of the tube and the liquid front moves from pore interior to the external surface. This is mainly during the constant-rate drying period. This model could capture only slow drying conditions and the metal migration

was through capillary flow and back diffusion. The Wasburn equation was used here to describe capillary flow rate. Metal deposition here was through adsorption only and precipitation was not considered. Li et al[16] studied the distribution of nickel distribution for a Ni/alumina system. In They developed a correlation where in the metal in solution could move only in one direction from support center to surface and opposite direction diffusion was neglected. Börnhorst et al [17]captured fundamental effects during drying in an existing pore network model by adaption of experimental pore structures and impregnation–drying conditions A good agreement of experiments with simulations was observed. Mahadevan et al.,[18] built a mathematical model to understand the flow-through drying process and to predict drying rates and the evolution of liquid saturation profiles. The model included the effects of gas compressibility and capillarity. Here, the capillary pressure gradients caused the liquid flow that leads to spreading of the saturation profile whereas the compressibility effects accounted for the evaporation into the saturated gas phase.

A recent work by Lekhal et al. used a Dusty Gas model and Darcy's law to describe the transport of gas and liquid phases respectively. [19-21] Transport of metal components was modeled using the Nernst-Planks equation, a Langmuir model was applied to describe the adsorption and desorption for the metal redistribution during the drying. Liu et al [5, 22] also talked about the effect of process parameters such as support permeability, diffusion, loading, adsorption, drying temperature etc, on the drying of nickel-alumina catalyst

support systems. They also incorporated the effect of film breakage into their drying model and it was seen to agree with experimental metal profiles. At the beginning of the drying process, the liquid phase is continuous and when evaporation proceeds the breakage of the liquid film throughout the porous structure takes place. The isolated domains in the liquid phase inhibit the liquid flux. At early drying stages, when convective flow dominates, the film breakage suppresses the formation of an egg-shell. If film breakage occurs at later stages of the drying process, an egg-shell profile is more favored due to lesser back diffusion [14, 15, 23].

Generally, for precious metals, precursors such as palladium or platinum, a low metal loading of about 0.1–1% mass of metal per mass of catalyst support is desired to optimize the process costs. However, for cheaper metals, such as nickel or copper, a higher metal loading (around 10–40% mass of metal per mass of catalyst support) is preferred to increase the space–time yield of the reactor. When these precursors have low melting points they melt and are mainly in molten phase at high drying temperatures (80^0C). Hence at higher loadings a different behavior is observed in the drying of nickel nitrate solution. [24] For high concentration the molten liquid could also directly be impregnated onto the support because of capillary forces and this method is commonly known as melt infiltration. [2, 23]

The capillary flow of solvent into the support can also be modified by altering the viscosity of the impregnating solution and this alters the liquid-air interface. [25] It was seen that the addition of organic molecules such as citric

acid or EDTA have previously been reported to change the viscosity of the impregnating solutions and this had an effect on the metal distribution. [26] Apart from these, at higher concentrations and temperature, the molten metal itself which is now in its liquid phase could alter the drying kinetics and metal distribution. In the work of Cherne et al [27] it was seen how theoretical models like Molecular Dynamics (MD) and the Embedded Atom Method (EAM) could be used to calculate the viscosity of liquid Nickel. Irving et al and Monnery et al presented several mixing equations and models to compute viscosities of solutions. [28, 29] The viscosities and densities were also derived experimentally for nickel nitrate solutions and mixture of solutions as a function of temperature. [28, 30, 31]

Liu et al [24] presented a theoretical model to predict post-drying metal distributions for a nickel nitrate hexahydrate-alumina system in both high and low concentration conditions which included temperature and concentration dependence on solution parameters like density, viscosity, surface tension. Models for viscosity and density of solution were adapted from a model presented by Marc Laliberté. [32-34] It was seen here that drying is much faster for low metal loading conditions than for high metal loading conditions which is because the water vapor pressure increased and the solution viscosity decreased with metal concentration. For a metal precursor with a high concentration and a low melting point, it was observed that the metal precursor is molten in the liquid phase during drying and the metal distribution after drying reached a nearly uniform profile when the system reached a certain

metal loading threshold. The drying model showed good agreement with the experimental data. [24] This model will be discussed in detail in the subsequent sections. In our work we have attempted to expand to other metal-support systems.

In this thesis, we analyzed a different metal precursor using the same type of support (as used in the model mentioned above). A detailed analysis on each of the metal and solution parameters led to us creating a reduced parameter model with fewer new parameters involved. This model could be used on different metal precursors without redoing multiple tedious, expensive and time consuming experiments. We tested this model using a new metal precursor and the results are presented in this thesis. For our experimental work, UV-Visible spectroscopy was used to measure the concentration of metal precursor in solution. Metal distributions in the supports were analyzed using a micro-X-Ray Fluorescence spectrometer.

2. Model and experimental setup

2.1. Model equations

In this work, we study the drying of a nickel precursor over an alumina support system, which is a widely used supported catalyst in processes like hydrogenation, hydrodesulphurization and steam reforming of hydrocarbons. [35-38] Nickel nitrate hexahydrate is a green crystalline solid which dissolves readily in water and is also an oxidizing agent because of the presence of nitrate ions. Higher stability and lower costs make nickel nitrate hexahydrate a better metal precursor in the catalyst industry when compared to its anhydrous form. One of the important properties of this material is its low melting point of 56^0C and hence it is usually in a molten state during drying. This has the potential to greatly affect the metal redistribution after drying. Similar phenomena could be also observed for other metal precursors with relatively lower melting points, such as cobalt nitrate hexahydrate, cobalt chloride hexahydrate and copper nitrate trihydrate. These materials are also often used in the catalyst industry. [24]

During the drying process of a supported catalyst several phenomena such as heat transfer from the hot gas to the wet support, solvent evaporation at the external surface, solvent convective flow toward the external surface, metal diffusion and adsorption inside the support occur simultaneously.

An accurate drying model must take into account the effect of all these phenomena. In our present work, we have optimized this model to make it

applicable to other metal systems on the same support. This is based on an analysis of the parameters affecting the distribution of metal in the catalyst support. This model is based on a model initially proposed by Lekhal et al. [19] and developed by Liu et al. [24] In this model, the following parameters have an impact on the drying process: the metal diffusion coefficient, the equilibrium constant of adsorption and desorption, the intrinsic permeability, the initial metal concentration in the solvent, the viscosity and density of metal solution, the volume ratio of metal, the drying temperature, the humidity of the drying air and film-breakage parameters. These parameters were determined for nickel nitrate hexahydrate on an alumina support.

There are two main assumptions considered in this model: (1) during the drying process, the metal concentration in the solution is below its maximum solubility; therefore, crystallization is not considered; (2) the equilibrium adsorption constant can be assumed to be constant during the drying process. These assumptions were made to arrive at a model that can simply yet accurately describe the important physical processes that take place during drying. This model can capture convective flow in the gas and liquid phases, metal convection, diffusion, adsorption on the porous support and heat transport. [5]

The following equations describe the drying process:

$$\frac{\partial}{\partial t}\left(\varepsilon_g C_{g,a}\right) = \frac{1}{r}\frac{\partial}{\partial r}\left(rN_{g,a}\right) \quad (1)$$

$$\frac{\partial}{\partial t}\left(\varepsilon_l C_{l,s} + \varepsilon_g C_{g,s}\right) = -\frac{1}{r}\frac{\partial}{\partial r}\left(\alpha r N_{l,s} + rN_{g,v}\right) \quad (2)$$

$$\frac{\partial}{\partial t}\left(\varepsilon_l C_{l,i}\right) = -\frac{1}{r}\frac{\partial}{\partial r}\left(\alpha r N_{l,i}\right) - \rho_s R_i \quad (3)$$

$$\frac{\partial}{\partial t}\left(C_{s,i}\right) = R_i, i = metal\ component \quad (4)$$

$$\frac{\partial}{\partial t}\left(\sum_{i=1}^{2}\varepsilon_g C_{g,i} h_{g,i} + \varepsilon_l C_{l,s} h_l + \rho_s h_s\right) = -\frac{1}{r}\frac{\partial}{\partial r}\left(\sum_{i=1}^{2} r N_{g,i} h_{g,i} + \alpha r N_{l,s} h_l - r\lambda\frac{\partial T}{\partial r}\right) \quad (5)$$

Equations (1) and (2) represent the mass balances of the drying medium (air) and the solvent (water) in a cylindrical support. Equations (3) and (4) represent the mass balances of the metal dissolved in the liquid and deposited on the support. Equation (5) is the energy balance. ε_g and ε_l are the volume fractions of the gas and liquid phases, $C_{g,a}$ (mol/m^3) and $C_{l,s}$ (mol/m^3) are the concentrations of the drying air and the liquid solvent, respectively. $C_{l,i}$ (mol/m^3) and $C_{s,i}$ (mol/kg) are the concentrations of the metal dissolved in the solvent and adsorbed on the support. $N_{g,a}$ (mol/m^2/s) and $N_{g,v}$ (mol/m^2/s) are the fluxes of the air and solvent vapor. $N_{l,s}$ (mol/m^2/s) and $N_{l,i}$ (mol/m^2/s) are the fluxes of the solvent and the dissolved metal. ρ_s (kg/m^3) is the apparent density of the porous support. R_i (mol/kg/s) represents the rate of metal adsorption, which is described using a Langmuir model [39-41].

$$R_i = k_{ads} C_{l,i}\left(C_{sat} - C_{s,i}\right) - k_{des} C_{s,i} \quad i = metal\ component \quad (6)$$

Where: k_{ads} (m^3/mol/s) and k_{des} (s^{-1}) are the adsorption and desorption constants of the metal component. C_{sat} (mol/kg) denotes the metal saturation concentration. In this model, it was assumed that adsorption is not the limiting parameter. Consequently, the adsorbed metal is in equilibrium with its dissolved precursor, and the equilibrium adsorption constant was calculated as $K_{eq} = k_{ads}/k_{des}$. However, the value of the equilibrium adsorption constant could change during drying [20]. In this work, we assume it to be a constant. $h_{g,i}$ (J/mol) represents the enthalpy of the air or solvent vapor. h_l (J/mol) and h_s (J/kg) denote the enthalpy of the liquid and solid. λ (J/(m/s/K)) is the effective thermal conductivity.

Film-breakage is an important phenomenon during drying. At the beginning of drying, the liquid phase is continuously distributed in the support. As evaporation proceeds, isolated domains are gradually formed in the liquid phase. Finally, the liquid is only found in the isolated domains. To consider the effect of film-breakage in our model, a factor α is added to the flux terms in equations (2), (3), and (5). Neimark et al [14] showed that film-breakage is related to the support pore structure and water content in the support. Therefore, for a given solid carrier, we assume that the film-breakage factor, α, is a function of the water volume fraction. [5]

$$\alpha = 1 \quad when\ \varepsilon_f \geq \alpha_1$$

$$\alpha = \frac{(\varepsilon_f - \alpha_2)}{(\alpha_1 - \alpha_2)} \quad when\ \alpha_1 > \varepsilon_f > \alpha_2$$

$$\alpha = 0 \quad when\ \varepsilon_f \leq \alpha_2 \tag{7}$$

Where: α_1 represents the water volume fraction when film breakage starts, and α_2 represents the water volume fraction when the solvent only exists in the isolated domains and the water flux completely stops. We assume that when the value of the water volume fraction is between α_1 and α_2, α linearly decreases with a decrease in the water volume fraction indicating that the flux in the liquid phase linearly decreases with a decrease in the water content. [5]

The gas-phase fluxes $N_{g,a}$ and $N_{g,v}$ are assumed to follow the dusty gas model (DGM), [42] which considers the effect of molecular diffusion, Knudsen diffusion, and viscous flow.

$$-\frac{P_g}{RT}\nabla x_{g,i} - \frac{x_{g,i}}{RT}\left(1 - \frac{KK_{g,eff}P_g}{\eta_g D_{Knud}}\right)\nabla P_g = \sum_{\substack{j=1 \\ j\neq i}}^{2} \frac{x_{gj}N_{g,i} - x_{g,i}N_{gj}}{D_{g,ij}} + \frac{N_{g,i}}{D_{Knud}} \tag{8}$$

$$N_{l,s} = -C_{l,s}\frac{KK_{l,eff}}{\eta_l}\nabla P_l \tag{9}$$

$$N_{l,i} = -C_{l,i}\frac{KK_{l,eff}}{\eta_l}\nabla P - \varepsilon_l D_{l,i}\nabla C_{l,i} - \varepsilon_l C_{l,i} Z_i D_{l,i}\frac{F}{RT}\nabla\phi_l, \quad i = metal\ component \tag{10}$$

where P_g (Pa) is the total gas pressure, R (8.314 J/(mol/K)) is the universal gas constant, T (K) is the temperature, $x_{g,i}$ represents the vapor or air mole fraction in the gas phase, $D_{g,ij}$ (m^2/s) and D_{Knud} (m^2/s) are the effective binary

and Knudsen diffusion coefficients, $K_{g,eff}$ is the intrinsic permeability of the gas phase, $K_{l,eff}$ is the relative permeability of the liquid phase, η_l (Pa s)is the viscosity of the liquid phase, K (m^2) represents the intrinsic permeability, P_l (Pa) is the liquid phase pressure, $D_{l,i}$ (m^2/s) is the effective diffusion coefficient of the dissolved metal, Z_i is the charge of the metal component, F (96,500 C/mol) is the Faraday constant and ϕ (V) represents the electrostatic potential. A detailed representation of this model is given in Liu et al. [5] The boundary conditions are the zero-flux conditions at the support center and the Neumann conditions at the support surface. [19] The resulting system of nonlinear partial differential equations is spatially discretized by a finite volume method. [43] The resulting set of ordinary differential equations is then solved by LIMEX, which is an efficient solver for highly stiff differential-algebraic equations. [44] In the drying model, the processing parameters include drying temperature, humidity in the drying air and air flux. For low metal concentrations, the following parameters have an impact on the drying process: the metal diffusion coefficient of metal precursor in the solvent, the equilibrium constant of adsorption and desorption, the kinetic adsorption constant, the saturation concentration of metal precursor on the support, the intrinsic permeability of the support, and film-breakage factors. Individual experiments were performed to determine these solution dependent parameters. [5, 24]

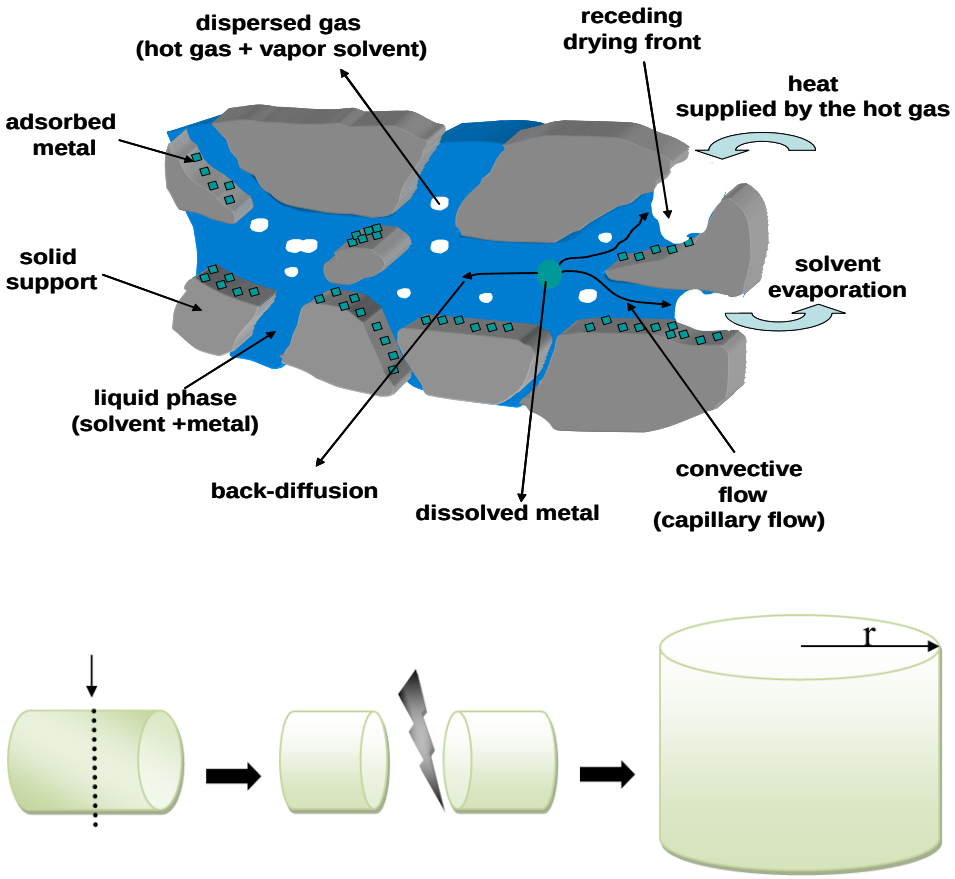

Figure 1: (Top) A pictorial respresentation of the transport of components within a catalyst support during drying. (Bottom) The description of the pellet cutting process, the circular cross-sectional area analyzed for experiements and the model

2.2. Experiment setup and parameter measurement

The aforementioned model was previously studied using several experiments for a nickel nitrate hexahydrate precursor over Alumina system. Our two main objectives for performing these experiments are: (1) To determine values for parameters pertaining to the metal solutions (2) To validate results generated by our model. When expanding to a new metal system, the parameters discussed here would have to be measured for the new metal.

Nickel nitrate hexahydrate powder (Sigma-Aldrich, St. Louis, MO, USA) was used as the metal precursor on cylindrical γ-alumina pellets as supports. These pellets were provided by Saint-Gobain Norpro (Stow, OH) and have a surface area of 200.7 m^2/g, length 10 mm and a diameter of 3mm. The void volume of these supports is 0.3 cm^3/g.

The experimental procedures in general follow these steps: (1) the supports (alumina) are heated overnight (12 hours) in an oven maintained at 120^0C. This allows for removal of any moisture present in them. (2) The supports are then immersed into the solution of metal precursor (nickel nitrate hexahydrate) at room temperature and left to impregnate until equilibrium is attained. (3) The supports are then dried at 80^0C in an oven. At this temperature, the nickel nitrate is in its molten phase (melting point is 56 ^{0}C). (4) The supports are cut into half in the radial direction and analyzed over a diametric line on the inner circular cross-section area.

Metal concentration in solution is measured using a UV-Visible spectrometer which gives absorbance of the solution. The peaks for a nickel nitrate solution are visible at 190nm. These will differ from metal to metal. The dried pellets are analyzed using a micro-X-Ray Fluorescence Spectrometer. [5] For our first objective - to predict a drying distribution using our model, several physical parameters have to be determined like viscosity, density, volume ratio of metal and adsorption constants. Independent experiments were developed to measure these parameters.

2.2.1 Volume ratio of metal

The volume ratio of metal gives us the volume occupied by the metal inside the solution as a function of metal concentration. This is an important parameter which varies from metal to metal. Fig. 2 shows the ratio of the volume of water added to reach a certain concentration to the total volume of the solution for different metal precursor concentrations. For example, to prepare a 100 ml of nickel nitrate solution of 1 M concentration, we add 84 ml of water to 29.079 g of nickel nitrate hexahydrate and the solution would add up to 100 ml. This implies that the rest of the volume is occupied by the metal, and the volume ratio would be 84 ml divided by 100 ml of solution = 0.84. A linear relationship was observed here. [5]

$$Volume\ of\ added\ water/total\ volume\ of\ solution = 1 - 0.1516 \times C_0 \qquad (12)$$

Where: C_o is the molar concentration of the nickel nitrate hexahydrate and 0.1516 is a regression factor (with units of inverse molar concentration). Once the temperature is above the melting point of nickel nitrate hexahydrate, the solute will melt and we can compute the maximum concentration of nickel nitrate hexahydrate by putting the left-hand side of eq. (12) equal to zero (no water added) and solve for C_o = (1/0.1516) M = 6.5 M.

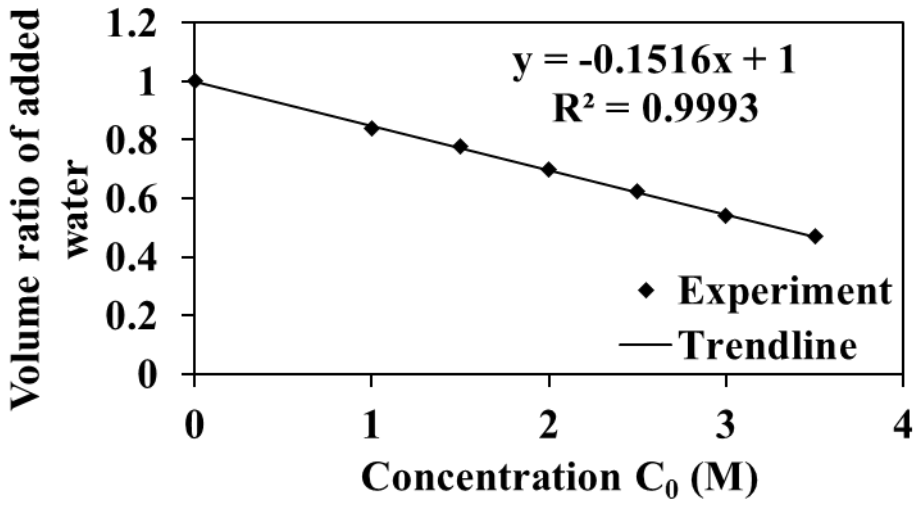

Figure 2: Variation of volume ratio of added water with nickel precursor concentration at room temperature

2.2.2 Vapor pressure

Raoult's Law was incorporated into our model to describe the effect of metal concentration on the vapor pressure of water. This is given by:

$$P = P_0(1 - X_i) \tag{13}$$

Where: P stands for the actual water vapor pressure, P_o stands for the vapor pressure of pure water and X_i is the mole fraction of solute ion. Raoult's law has been widely used to describe vapor pressure in many salt-water systems. The driving force for evaporation greatly reduces with an increase in concentration i.e., for a 4.0M solution, P/P_0 equals 0.65. A factor '3' is added while calculating X_i to consider three components of solute species, one nickel and two nitrate ions.

2.2.3 Density, viscosity and surface tension

Fig. 3 shows the variation of the solution density with the nickel nitrate concentration at room temperature. The dots represent experimental data and the solid line represents theoretical results. [5] To predict the density of metal solution (nickel nitrate hexahydrate), a formula originally proposed by Marc and Cooper (2004) is used in this model:

$$\rho_l(kg \times m^{-3}) = \frac{1}{(w_w/\rho_w) + (w_{Ni}/\rho_{Ni})}$$

$$\rho_{Ni}(kg \times m^{-3}) = \frac{(c_0 w_{Ni} + c_1)\exp(0.000001(T + c_4)^2)}{w_{Ni} + c_2 + c_3 T} \quad (14)$$

Where c_0 =1.17x10^{-5} kg/m^3; c_1 = 8.78 x 10^{-6} kg/m^3; c_3 = 0.00624^{0}C^{-1}; c_4 = 4369.047^{0}C^{-1} and ρ_w is the density of water, ρ_{Ni} is the density of nickel nitrate in the solution, w_w and w_{Ni} are the weight ratios of water and nickel nitrate in the solution, and c_0–c_4 are empirical constants for nickel nitrate hexahydrate. [33, 34] In the formula, the solution density is a function of the temperature and the nickel nitrate concentration. It can be seen that the solution density increases with an increase in the nickel nitrate concentration. We also observe that the fitted model and the experimental data have a good agreement.

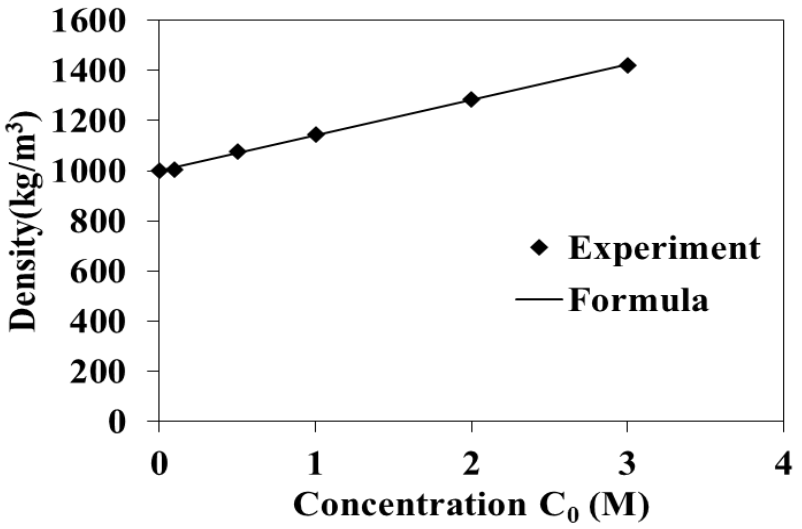

Figure 3: Variation of solution density with nickel precursor concentration at room temperature

The viscosity of the solution was measured using a rheometer. The nickel nitrate hexahydrate solution viscosity increases with increasing concentration of nickel nitrate (see Fig. 4). A formula proposed by Marc (2007) [32] is used in this model to describe the variation of the solution viscosity with respect to the temperature and nickel nitrate concentration.

$$ln\eta_1 = w_w ln\eta_1 + w_{Ni} ln\eta_{Ni}$$

$$\eta_w(mPa\ s) = \frac{T(°C) + 246}{(0.05594T + 5.2842)T + 137.37}$$

$$\eta_{Ni}(mPa\ s) = \frac{\exp((\nu_1 {w_{Ni}}^{\nu_2} + \nu_3)/(\nu_4 T + 1))}{\nu_5 {w_{Ni}}^{\nu_6} + 1} \quad (15)$$

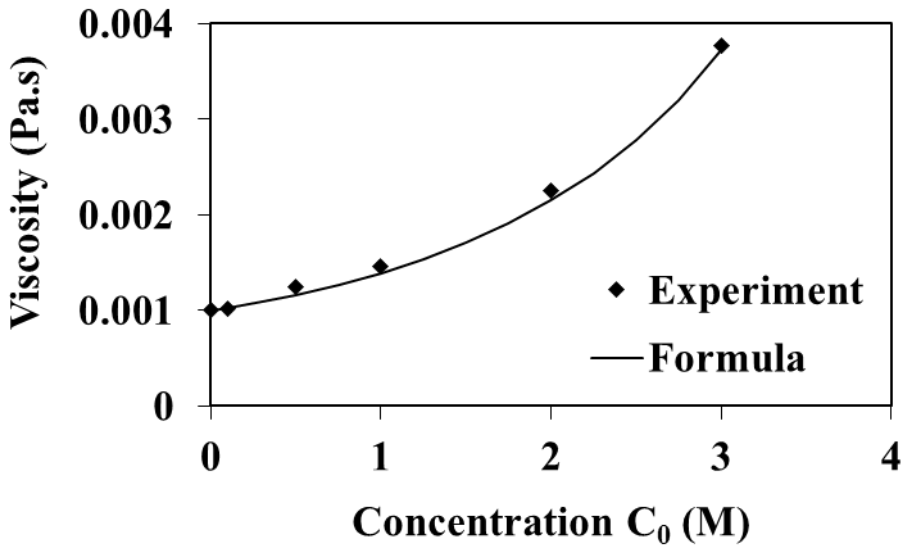

Figure 4: Variation of the solution viscosity with the nickel precursor concentration at room temperature

The surface tension on the nickel nitrate hexahydrate solution was measured using a pendant drop test [45]. In this test, the gravitational force of a droplet is balanced by the force of surface tension. We noted that a linear relationship was observed between the concentration of nickel nitrate hexahydrate and solution surface tension. The slope here was noticeably small indicating a relatively low effect of solution surface tension on the concentration of nickel nitrate. The model was fit to our experimental data using regression (see Fig. 5). This equation was used to calculate the surface tension for different concentrations of nickel nitrate hexahydrate.

$$Solution\ Surface\ Tension, \gamma\ (N/m) = 0.0033C_0 + 0.072 \quad (16)$$

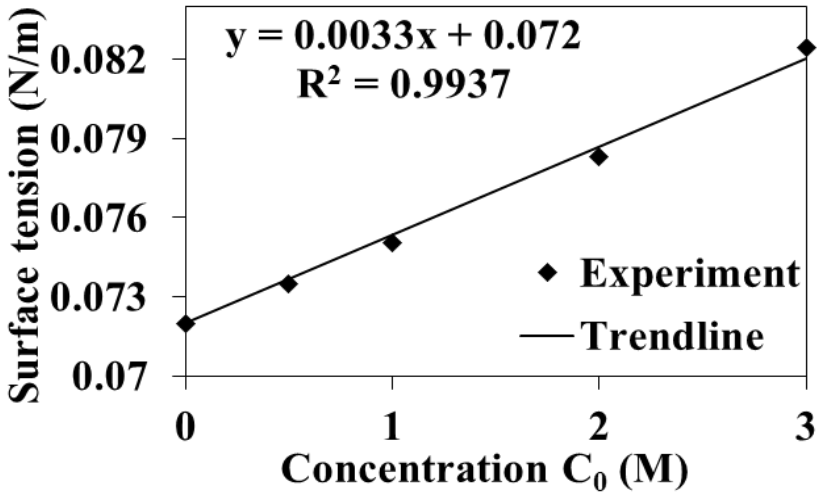

Figure 5: Variation of the solution surface tension with the nickel precursor concentration at room temperature

2.2.4 Adsorption- desorption constants

The adsorption behavior of metal onto the support was determined using a Langmuir adsorption model. We assume the nickel over alumina system follows a Langmuir adsorption model (Eq. (6))

2.2.4.1 Adsorption equilibrium constant (K_{eq}), saturation concentration (C_{sat})

For a nickel nitrate hexahydrate over alumina system, a simple experiment was performed and the system was allowed to attain equilibrium. 100 ml solutions of nickel nitrate hexahydrate were prepared and 1 g of preheated support was added into each of these solutions. Solutions of 6 different concentrations: 0.01 M, 0.02 M, 0.04 M, 0.06 M, 0.08 M, and 0.1 M were prepared with the pH maintained at 6.5 at room temperature and pressure. The system was allowed to attain equilibrium. The nickel nitrate concentration in

these solutions was then measured using a UV-Visible spectrometer with a peak observed at 190 nm. The solutions were tested on the UV-Vis until equilibrium was attained, with the assumption that equilibrium is attained is when there is no appreciable difference in the absorbance of the solution over time. Absorbance is correlated to concentration using a calibration with solutions of known concentrations. A linear relationship was observed (see fig. 6):

$$C_{Ni} = 0.0878A_{uv} \tag{17}$$

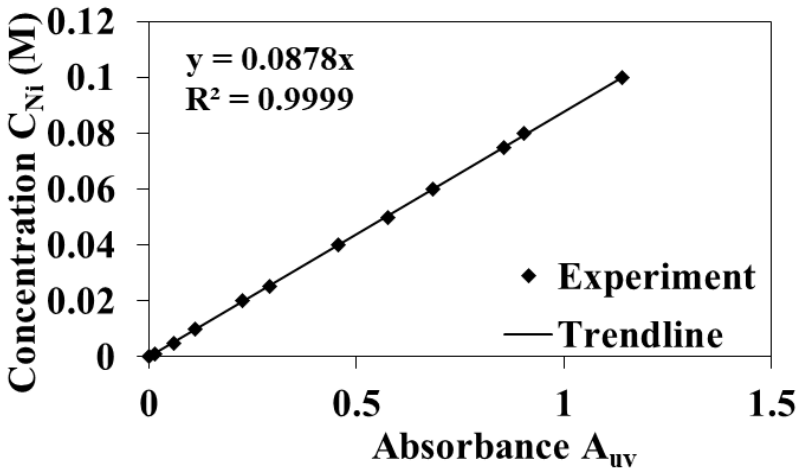

Figure 6: Variation of absorbance with nickel nitrate hexahydrate solution concentration measured using a UV-Visible spectrometer at room temperature

When equilibrium is attained the total rate of absorption is equal to zero and Eq. (6) can be rewritten as

$$\frac{1}{C_{eq}} = \frac{1}{C_{sat}K_{eq}}\left(\frac{1}{C_{s,i}}\right) + \frac{1}{C_{sat}} \tag{18}$$

The concentration of metal adsorbed on support ($C_{s,i}$) can be calculated by a mass balance on the system. The difference between the initial concentration in solution and after adsorption gives us the amount of metal adsorbed onto the support. From the above equation a linear correlation is observed between $1/C_{eq}$ and $1/C_{s,i}$ and the values of C_{sat} and K_{eq} are obtained from the line intercept and slope (see fig.7). Using Eq. (18), we obtained C_{sat} = 0.3 mol/kg and K_{eq} = 0.2 m^3/mol. Here we assume our model obeys the linear relation obtained in the given range. This is because we had to optimize our range to the given set of values where in we get a linear relationship. We were subject to this range because of limits of detection of our UV-Visible spectrometer

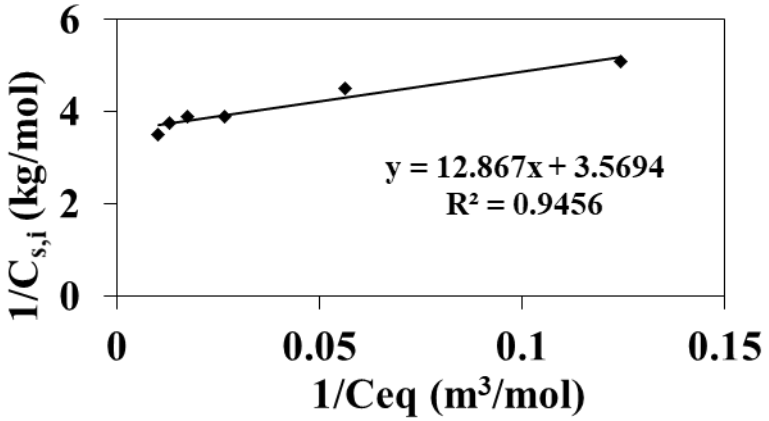

Figure 7: Measurement of adsorption constants (K_{eq} and C_{sat}) for nickel nitrate hexahydrate over alumina supports using a UV-Visible spectrometer at room temperature

2.2.4.2 Kinetic adsorption constant

For the kinetic adsorption constant, we consider the initial stages of adsorption where the effect of desorption can be neglected. Hence, the adsorption of metal on the support is the solely responsible for a drop in concentration in solution. Eq (6) can be then rewritten as:

$$\frac{dC_o}{dt} = -k_{ads}\,\rho\,C_{sat}\,C_o \qquad (19)$$

Where: C_o represents the initial metal concentration in the solution. [16, 40] When we plot dC_o/dt versus C_o, a straight line is observed and the value of the slope gives us the kinetic adsorption constant k_{ads}. A simple experiment was performed, where five samples of nickel nitrate hexahydrate were prepared with concentrations 0.01, 0.02, 0.03, 0.04 and 0.05 M, the pH maintained at 6.5 and the samples kept at room temperature. 1 g of supports were prepared for impregnation in the solutions. In an attempt to reduce diffusion effects during impregnation, the supports were ground into a fine powder with the particle sizes between 150 to 250µm. Larger particles were sieved out and the finer ones were washed away using water. The powdered supports were then dried in the oven maintained at 120°C for 12 hours before impregnation. After impregnation was initiated, the metal concentration was measured at an interval of 10 minutes during the first hour of impregnation and every one hour there upon, until equilibrium was attained.

This certain time limit was taken as a period corresponding to no desorption, precisely because equilibrium attainment would take 24 hours or more for this

system. The value of dC_o/dt was then calculated by plotting dC_o/dt versus C_o and the kinetic adsorption constant, k_{ads}, was then found to be equal to 6.5×10^{-5} $m^3/mol/s$.

3. Results and discussion

The results are presented as follows: 1. Comparison of the present high concentration model to experiments 2. Comparison of the high concentration model to the low concentration model and 3. Development of the reduced parameter model based on this high concentration model.

3.1 High concentration model comparison with experiments

Experiments were performed on a nickel nitrate hexahydrate- alumina system to strike a comparison with the predictions from this model. Supports used here were of the specifications described in the section 2.1. The supports were dried overnight in an oven maintained at 120^0C prior to impregnation. Nickel nitrate hexahydrate solutions were prepared for different concentrations and the supports were left to impregnate in them until equilibrium is attained. The supports are then dried in an oven maintained at 80^0C until the drying end point is attained. The dried supports are cut into half in the radial direction and the inner circular cross-sectional area is analyzed using a micro-X-ray Fluorescence Spectrometer (refer fig.8,10). The linescan feature of the micro-XRF is used here, where in the X-ray beam is focused on a line which is divided into a specific number of points. The Rh tube X-ray beam voltage is maintained 50 KV and the current at 600uA. The line scan was performed under vacuum and on a diametrical line on the inner cross sectional area. The intensities measured from the X-ray beam are quantified into mass percentages. The metal distribution on the catalyst support is represented by

the mass of nickel normalized by the mass of alumina. This distribution is plotted as a function of dimensionless distance over a diametric line on the cross-sectional area of the dried support. We observed a good correlation with our experiments and the high concentration model for a different set of concentrations. In fig. 9 it can be seen how the experimental profiles and predictions generated by the model show appreciable agreement with each other. For the two concentrations shown here three different supports were dried and analyzed. The average of the three supports with error bars were plotted against the simulation results.

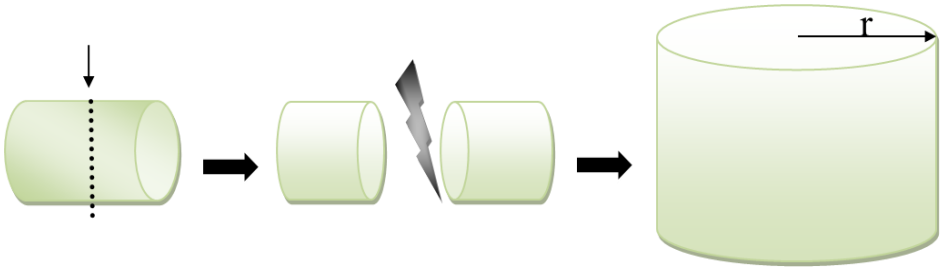

Figure 8: Steps of the catalyst support cutting process describing the circular cross-sectional area analyzed for experiments.

These experiments were also performed earlier on another instrument and were compared with the simulation. These experiments were performed on this new micro-XRF spectrometer to strike a comparison with the old instrument and ensure that we were getting the right metal distribution profiles.

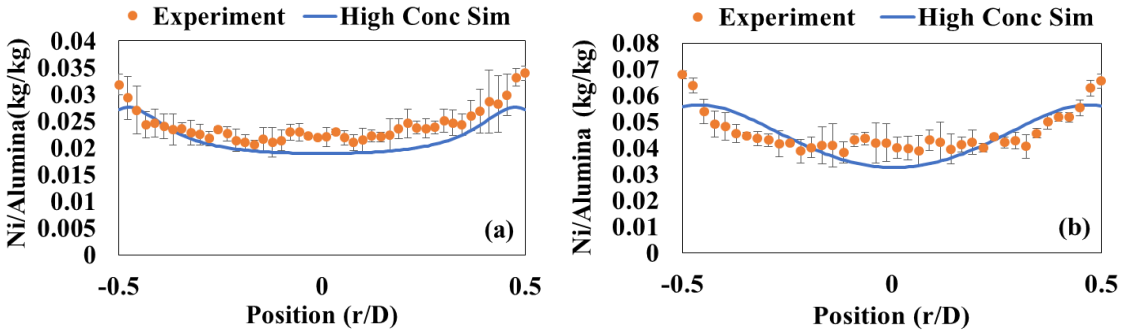

Figure 9 : Post drying metal distributions generated from high concentration model compared to experimental profiles for nickel nitrate hexahydrate on γ-alumina. Results show distribution from surface of the support to surface of the support, dried at 80^0C and uniform initial condition for two different metal loadings (a) 0.1 M (b) 0.5 M

Figure 10 : M4 Tornado micro-X-ray spectrometer by Bruker accompanied with a vacuum pump

3.2 High concentration model comparison

The model developed in previous work [5] is only applicable to low concentrations since we assumed that the properties of the metal precursor

solution were only determined by water and were not affected by the variation of metal concentration during drying. In the high concentration model studied here [24] the effect of solution properties was taken into account. Several other parameters that were determined in section 2.2 were incorporated into the model. The effect of nickel nitrate hexahydrate concentration on the solution density, solution viscosity, vapor pressure of water and solution surface tension were considered in this drying model. In the present work, we hold the drying temperature at 80^0C which is above the melting point of nickel nitrate hexahydrate (56^0C) and begin drying with a uniform initial condition (metal is distributed uniformly in the support before the drying begins). We then compared the two models to the experimental results obtained.

The metal distribution on the catalyst support is represented as the mass of nickel normalized by the mass of alumina. This distribution is plotted as a function of distance over a diametric line on the cross-sectional area of the dried support (refer Fig. 11). For the 3.0 M case the result generated from the high concentration model fits better with the experimental results when compared to the low concentration model. The low concentration model predicts a pronounced egg shell metal distribution in comparison to the uniform distribution predicted by the high concentration model. At this high concentration and drying temperature, most of the liquid is molten metal and the effect of the capillary force is strong enough to generate liquid flow inside the support. [24] For the case of a 1.0 M nickel solution we again see that the egg shell distribution predicted by the high concentration model fits better

with the experimentally obtained profiles when compared to the low concentration model.

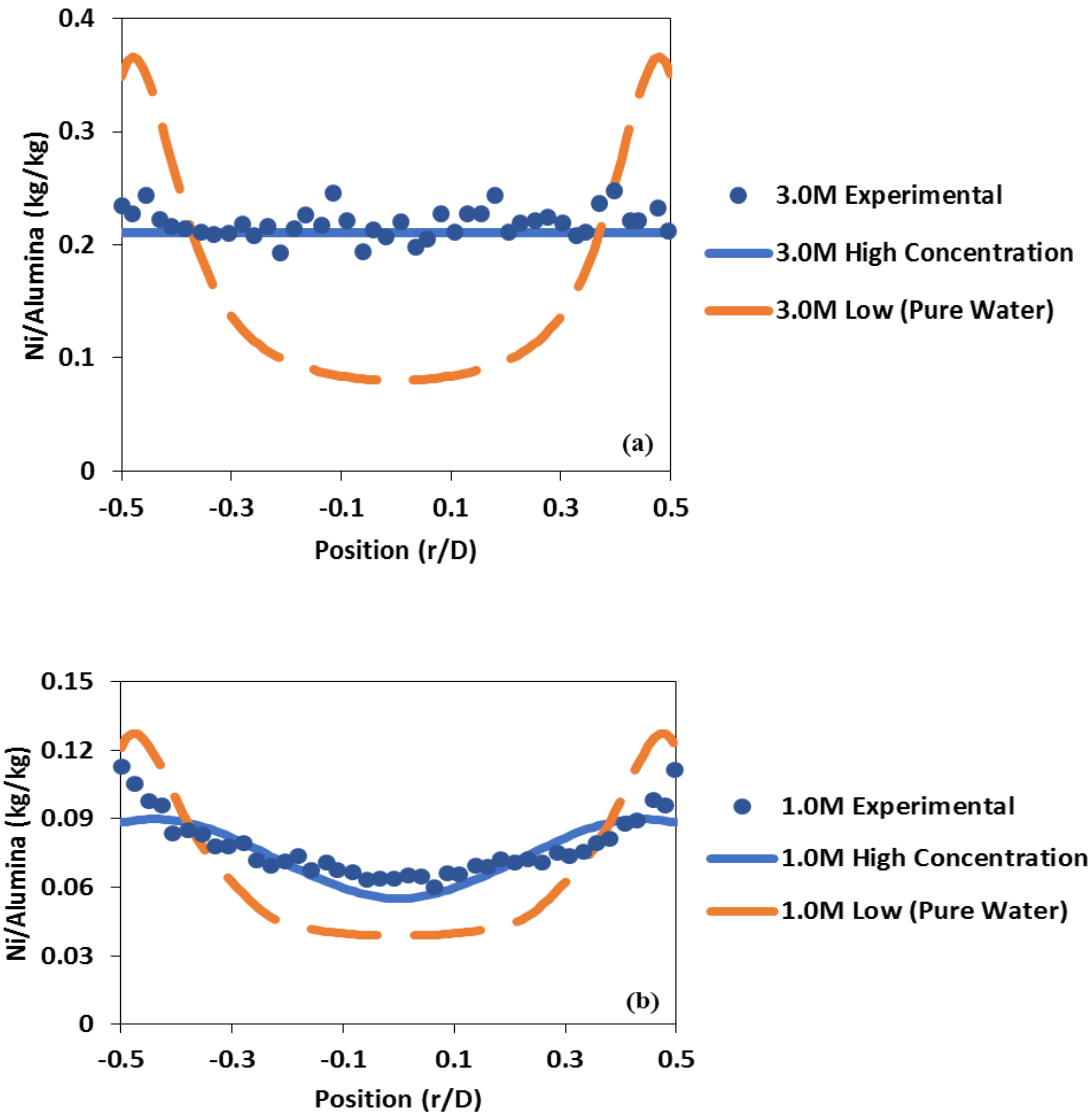

Figure 11 : Post drying metal distributions generated from high concentration model and low concentration (pure water) model compared to experimental profiles for nickel nitrate hexahydrate on γ-alumina. Results show distribution from surface to surface of the support, dried at 80 ^{0}C and uniform initial condition for two different metal loadings (a) 3.0 M and (b) 1.0 M

3.3 Reduced parameter model

The above mentioned high concentration model is built on properties and experiments using nickel nitrate hexahydrate as the metal precursor. To make the model applicable to other metal-support systems, all of the aforementioned solution parameters would have to be measured again for the new metal making it a tedious and lengthy task. In an attempt to reduce the burden of time consuming experiments, we performed a detailed analysis investigating the effect of every parameter on the post drying metal distribution for a uniform initial condition. The analysis was performed by initially considering just the pure water solution property effects on the model, then adding in the concentration dependent solution properties, mentioned in section 2.2, one by one and comparing the simulation results at each step to the full high concentration model results. This new model is called the reduced parameter model.

3.3.1 Metal solution properties

Effect of volume ratio of metal (VRM): Initially, we included only the volume ratio of metal for nickel nitrate hexahydrate, keeping other properties unchanged (pure water) and simulation results were compared to those of the original high concentration model. Fig. 12 shows a comparison of simulation results for post drying metal distributions from the high concentration model to the reduced parameter model (VRM) for nickel nitrate hexahydrate on γ-alumina. Two different metal loadings were tested - 3.0 M and 1.0 M. In this

figure, the high VRM simulation ended prematurely due to a solver crash from an unrealistically high drying rate due to an unrealistically high vapor pressure.

Inclusion of the volume ratio of metal generally leads to more uniform metal distributions. Due to film breakage, the metal flux becomes zero when the liquid volume fraction (which includes both water and metal) is less than 0.013. The volume ratio of metal for higher concentrations is always greater than 0.013, thus the metal flux never stops, allowing continued back-diffusion from the pellet surface and leading to a uniform profile. This shows us that the effect of the volume ratio of metal is important to generate these uniform profiles at higher concentrations (3.0 M).

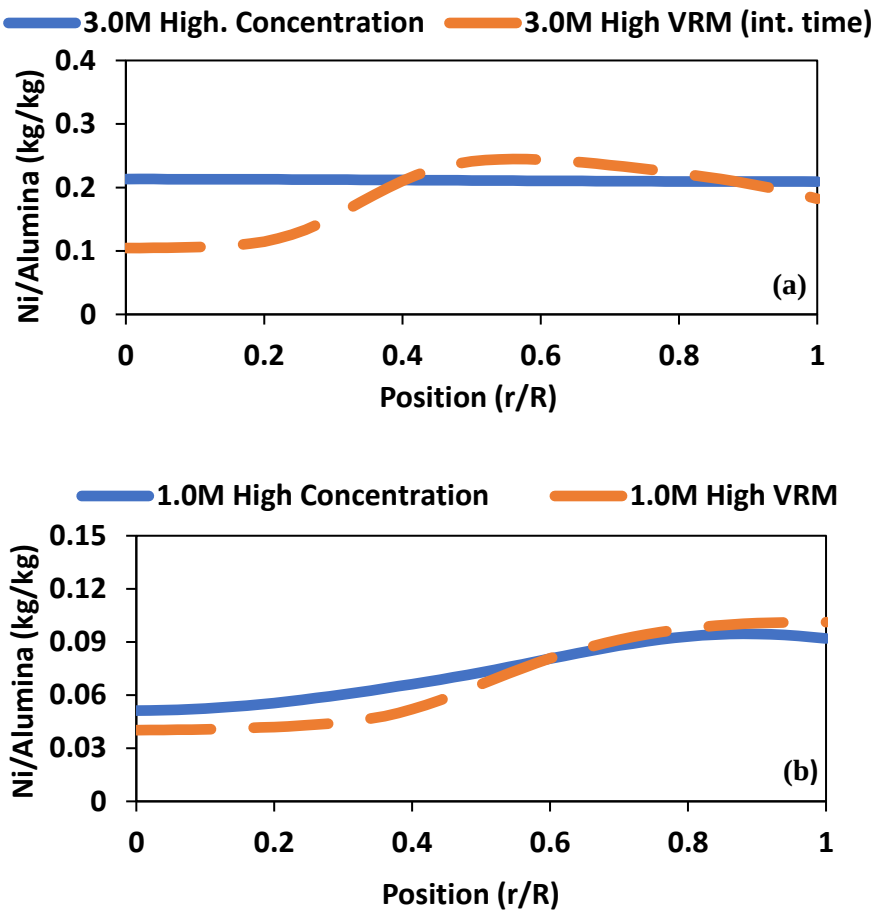

Figure 12: Simulation results comparing post drying metal distributions from the high concentration model to the reduced parameter model (VRM only) for nickel nitrate hexahydrate on γ-alumina. Results show distribution from center of the support to surface of the support, dried at 80 ^{0}C and uniform initial condition for two different metal loadings (a) 3.0 M and (b) 1.0 M. Note: The 3.0 M High VRM simulation ended prematurely due to a solver crash from an unrealistically high drying rate due to an unrealistically high vapor pressure. Note: The 3.0 M high VRM simulation ended prematurely due to a solver crash from an unrealistically high drying rate due to an unrealistically high vapor pressure

Effect of vapor pressure (VP): The figure below (Fig. 13) describes simulation results comparing post drying metal distributions from the high

concentration model to the reduced parameter model (VRM+VP) including the volume ratio of metal and vapor pressure for nickel nitrate hexahydrate over γ-alumina. Again, two different metal loadings were tested, 3.0 M and 1.0 M. With the inclusion of vapor pressure into the reduced parameter model, we see an appreciably better agreement with the high concentration model at both concentrations, 3.0 M and 1.0 M. It can also be observed from equation 13, that the vapor pressure is a concentration dependent property and greatly affects the rate of drying.

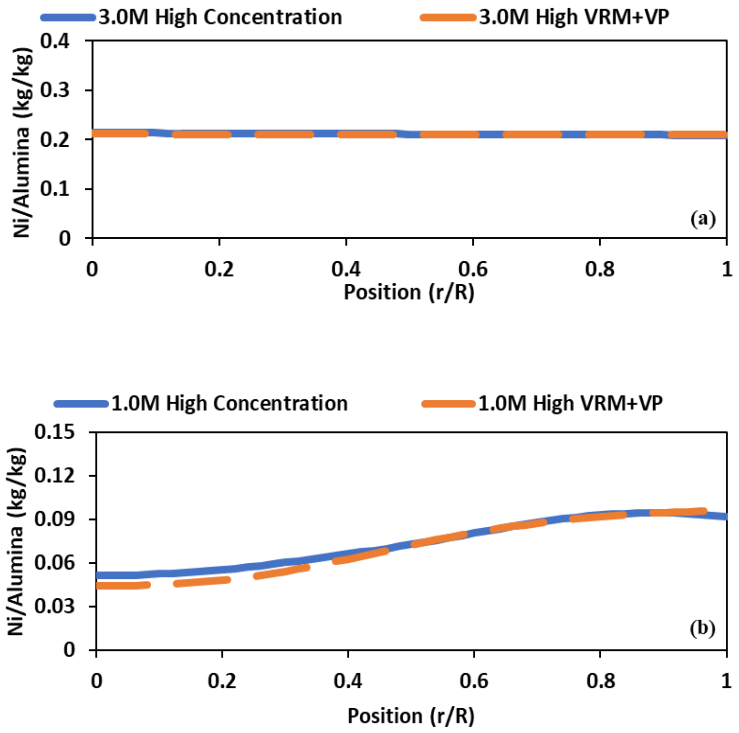

Figure 13: Simulation results comparing post drying metal distributions from the high concentration model to the reduced parameter model (VRM+VP) for nickel nitrate hexahydrate on γ-alumina. Results show distribution from center of the support to surface of the support, dried at 80^0C and uniform initial condition for two different metal loadings (a) 3.0 M and (b) 1.0 M

Effect of density, viscosity and surface tension: We included the density, viscosity and surface tension of the solution, one by one, into the model along with the volume ratio of metal and vapor pressure. The figure below (Fig. 14) describes the simulation results comparing post drying metal distributions from the original high concentration model to the reduced parameter model including the effect of volume ratio of metal, vapor pressure and density of metal (VRM+VP+ Density). With the inclusion of experimentally determined density for nickel nitrate solution, a good fit was observed with the high concentration model. However, it was also observed that the inclusion of density (together with the volume ratio of metal and vapor pressure) only lead to slightly better agreement with the high concentration model (refer fig. 14) when compared to the previous case (refer fig. 13). As already discussed, the metal distribution for the reduced parameter model fits reasonably well with the high concentration model with the inclusion of the volume ratio of metal and vapor pressure only (refer fig. 13). Further work was carried out by including the viscosity and surface tension for the nickel nitrate hexahydrate solution into the reduced parameter model. The two parameters had a negligible difference on the post drying metal profiles (not shown here) when compared to the previous case (refer fig.13 and 14).

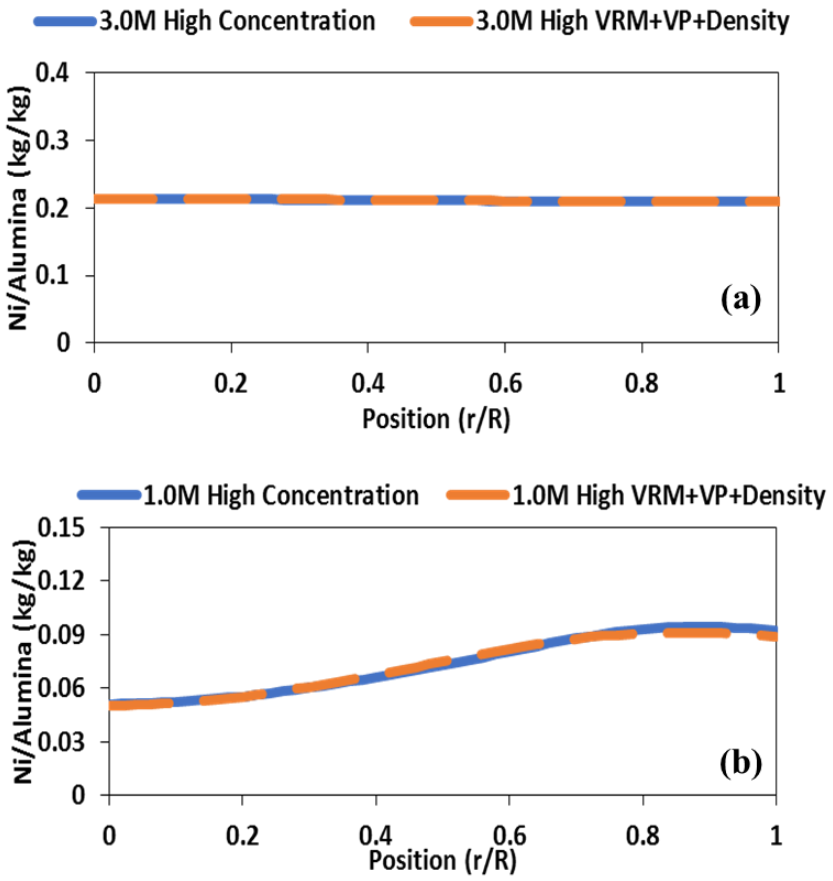

Figure 14: Simulation results comparing post drying metal distributions from the high concentration model to the reduced parameter model (VRM+VP+ Density) for nickel nitrate hexahydrate over γ-Alumina. Results show distribution from center of the support to surface of the support, dried at 80^0C and uniform initial condition for two different metal loadings (a) 3.0 M and (b) 1.0 M.

Comparison of three cases: The three cases mentioned above were compared to the high concentration model in Fig. 15. The water volume fraction results generated from the simulations were plotted against drying time for the three cases – volume ratio of metal (VRM), volume ratio of metal and vapor pressure (VRM+VP), volume ratio of metal, vapor pressure and density of solution

(VRM+VP+Density). It can be seen in Fig. 15 that the drying rate is decreased when Raoult's Law (VRM+VP) is included for the nickel nitrate hexahydrate i.e. the vapor pressure decreases as the concentration of the nickel nitrate hexahydrate increases. As drying proceeds the concentration of nickel nitrate hexahydrate increases leading to a lower vapor pressure and lower drying rate. This allows more time for back diffusion to occur, yielding more uniform metal distributions. It can be observed that just by including the volume ratio of metal and vapor pressure (VRM+VP) a fairly close match to the high concentration model is obtained. Further addition of the density of the solution into the model (VRM+VP+Density) leads to results that are almost indistinguishable from the high concentration model.

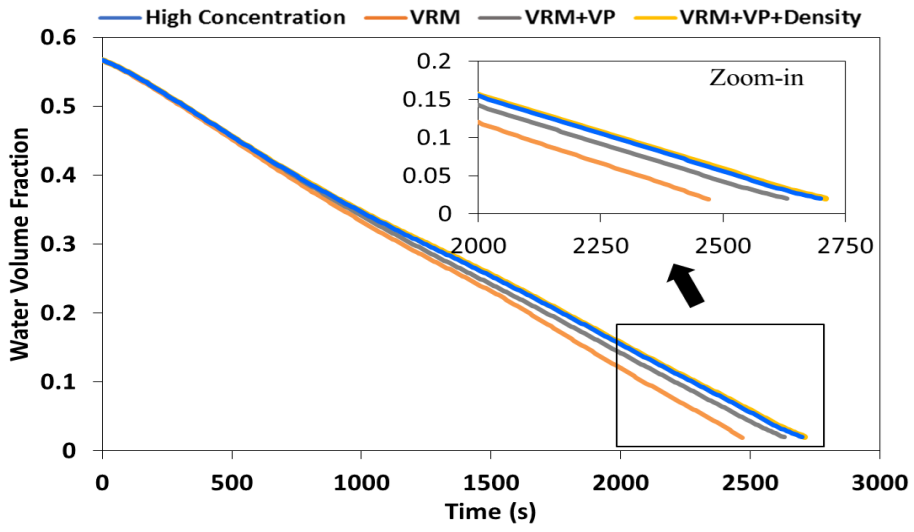

Figure 15: Simulation results from high concentration model compared to different reduced parameter models depicting the drop in water volume fraction with time

3.3.2 Adsorption parameters

Next, we moved on to a detailed analysis on the parameters governing the low concentration model and analyzed their effect on metal redistribution after drying. The parameters that are affected by the metal precursor would be the kinetic equilibrium constant (k_{eq}), the kinetic adsorption constant and (k_{ads}), the saturation concentration (C_{sat}) and the diffusion co-efficient (diffusivity). We understand from the previous work by Liu et al [5] how the initial concentration of the metal solution could have a strong effect on the metal loading and could affect distribution. We hence analyzed how the metal distribution would vary on varying these parameters since, a new metal would have a different adsorption strength. Hence we performed a detailed analysis of the adsorption parameters mentioned in section 2.2.5 to observe how they affect the post drying metal distributions. The metal adsorption onto the support is given by the Langmuir adsorption model. This gives us the rate of metal adsorption on alumina as a function of three important parameters: kinetic equilibrium constant, kinetic adsorption constant and saturation concentration.

Effect of kinetic equilibrium constant (K_{eq}): The kinetic equilibrium constant for nickel nitrate hexahydrate on γ-Alumina determined from experimental data is 0.2 m^3/mol (section 2.2.4.1). We varied this constant to a magnitude ten times higher and lower than the original value i.e., 2.0 m^3/mol and 0.02 m^3/mol respectively. The figure below (fig. 16) shows how the metal distribution is affected by these K_{eq} values. When drying from a uniform initial

condition, the final metal profile becomes more sensitive to the equilibrium adsorption constant as the impregnation concentration decreases. This is because the metal adsorption is driven by equilibrium at lower concentrations and by saturation concentration of metal at higher concentrations. The model begins drying from a uniform initial condition, where in the system has reached equilibrium. At lower concentrations the amount of metal adsorbed on the support is strongly controlled by the equilibrium concentration. In addition to that, it is assumed that there is a large enough amount of solution, which after impregnation does not lead to a drop in concentration. This condition pertains to wet impregnation system. Together, this leads to the initial condition where in the total amount of metal equals to the sum of free metal in solution (equal to the initial concentration of impregnation solution) and bound metal adsorbed on support (pertaining to equilibrium concentration).

Due to these factors there is difference in the total amount of metal adsorbed on the support for different values of equilibrium concentration even when the initial concentration of impregnating solution is kept constant. Hence a difference is observed after drying too.

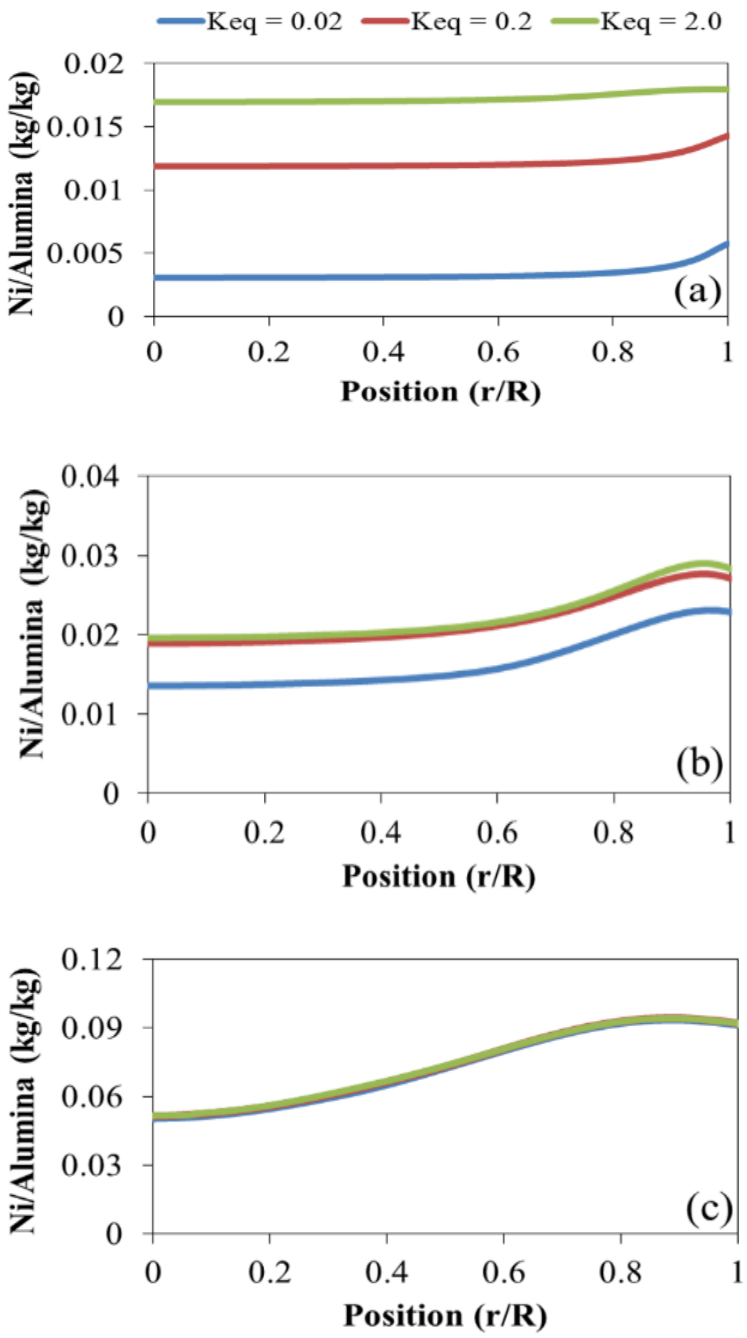

Figure 16: Reduced parameter model simulation results comparing post drying metal distributions for different kinetic equilibrium constant values of nickel nitrate hexahydrate over γ-Alumina. Results show distribution from center of the support to surface of the support, dried at 80^0C and a uniform initial condition for different metal loadings (a) 0.01 M, (b) 0.1 M and (c) 1.0 M.

Effect of kinetic adsorption constant (k_{ads}): A similar analysis was performed on the kinetic adsorption constant of nickel nitrate hexahydrate on γ-alumina. This value was obtained as 6.5 x 10^{-5} m^3/mol from experiments described in section 2.2.4.2. We varied the constant to a magnitude ten times higher and lower i.e., 6.5 x10^{-4} m^3/mol and 6.5 x 10^{-6} m^3/mol respectively. It can be seen in fig. 17, the different values of k_{ads} did not have any significant effect on the metal distribution at both low and high concentrations.

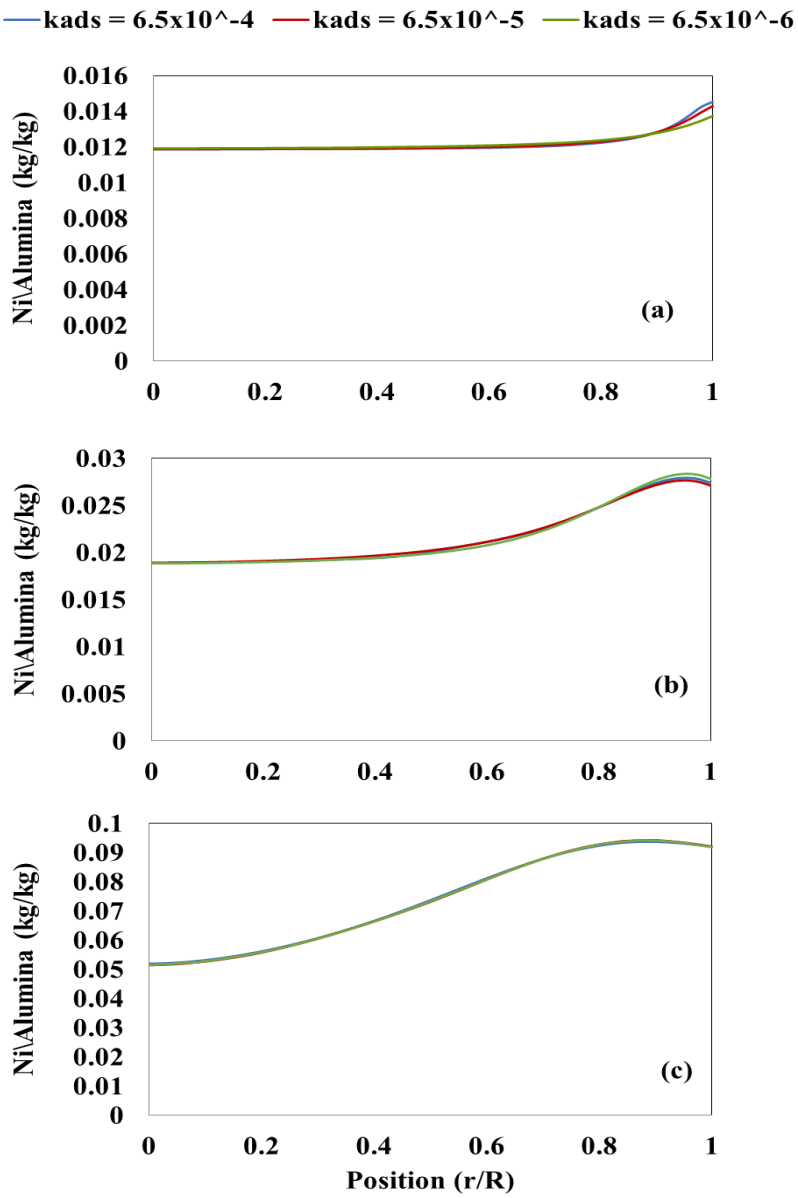

Figure 17: Reduced parameter model simulation results comparing post drying metal distributions for different kinetic adsorption constant values of nickel nitrate hexahydrate over γ-alumina. Results show distribution from center of the support to surface of the support, dried at 80^0C and a uniform initial condition for different metal loadings (a) 0.01 M, (b) 0.1 M and (c) 1.0 M

Effect of saturation concentration (C_{sat}): The saturation concentration of metal increases with an increase in initial concentration of metal in solution, as observed in section 2.2.4.1. An analysis was performed for three different concentrations of nickel nitrate hexahydrate i.e., 0.01 M, 0.1 M and 1.0 M. The saturation concentration from experiments described in section 2.2.4.1 was obtained as 0.3 kg/mol. The value was varied to a magnitude 10 times higher and lower i.e., 3.0 and 0.03 kg/mol respectively. The post drying metal distributions are significantly affected on varying these values (see fig. 18). The model begins drying from a uniform initial condition, where in the system has reached equilibrium. The amount of metal adsorbed on the support is strongly controlled by the saturation concentration. In addition to that, it is assumed that there is a large enough amount of solution, which after impregnation does not lead to a drop in concentration. This condition pertains to wet impregnation system. Together, this leads to the initial condition where in the total amount of metal equals to the sum of free metal in solution (equal to the initial concentration of impregnation solution) and bound metal adsorbed on support (pertaining to saturation concentration).

Due to these factors there is difference in the total amount of metal adsorbed on the support for different values of saturation concentration even when the initial concentration of impregnating solution is kept constant. Hence a difference is observed after drying too.

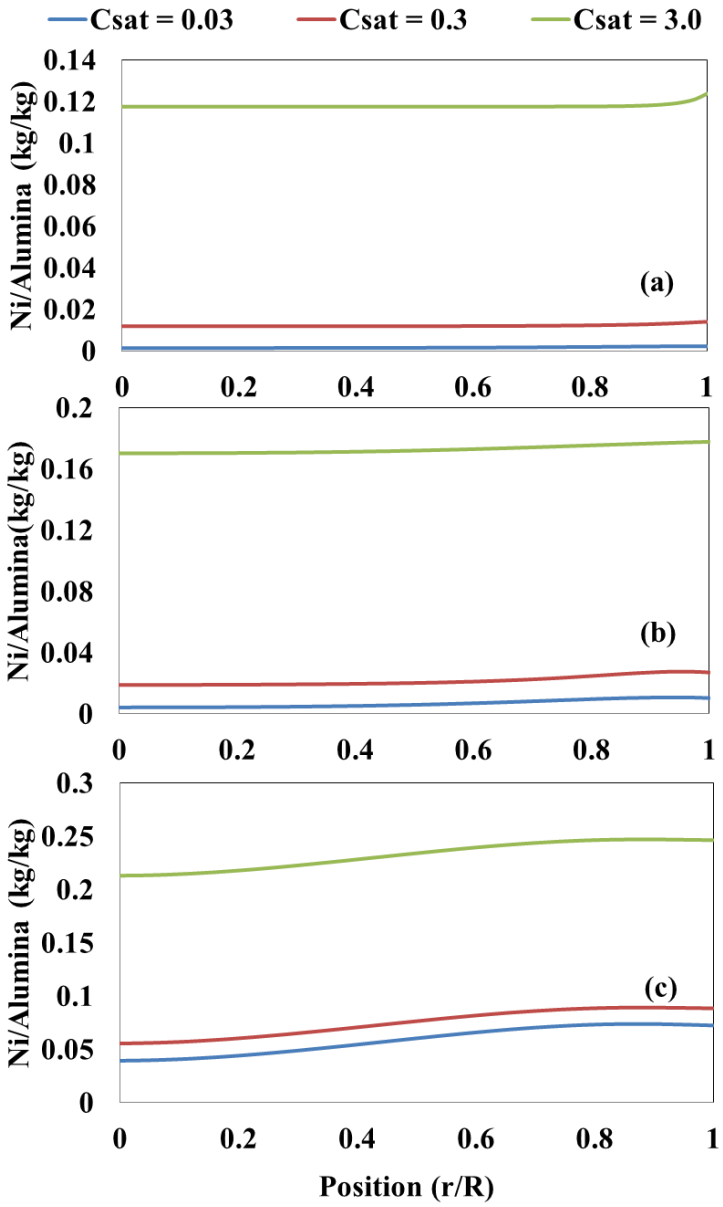

Figure 18: Reduced parameter model simulation results comparing post drying metal distributions for different saturation concentration values of nickel nitrate hexahydrate over γ-Alumina. Results show distribution from center of the support to surface of the support, dried at 80^0C and a uniform initial condition for different metal loadings (a) 0.01 M, (b) 0.1 M and (c) 1.0 M

Effect of diffusivity: The diffusion co-efficient of nickel nitrate hydrate is obtained as $6.6x10^{-10}$ m^2/s from literature [46]. Again a similar analysis was performed for three different concentrations of nickel nitrate hexahydrate i.e., 0.01 M, 0.1 M and 1.0 M. The diffusion co-efficient was varied by a magnitude ten times higher and lower i.e., $6.6x10^{-9}$ and $6.6x10^{-11}$ m^2/s. The diffusion coefficient has as increasing effect with an increase in concentration. It is also observed that increasing the diffusion co-efficient led to more uniform metal profiles and vice versa (see Fig.19).

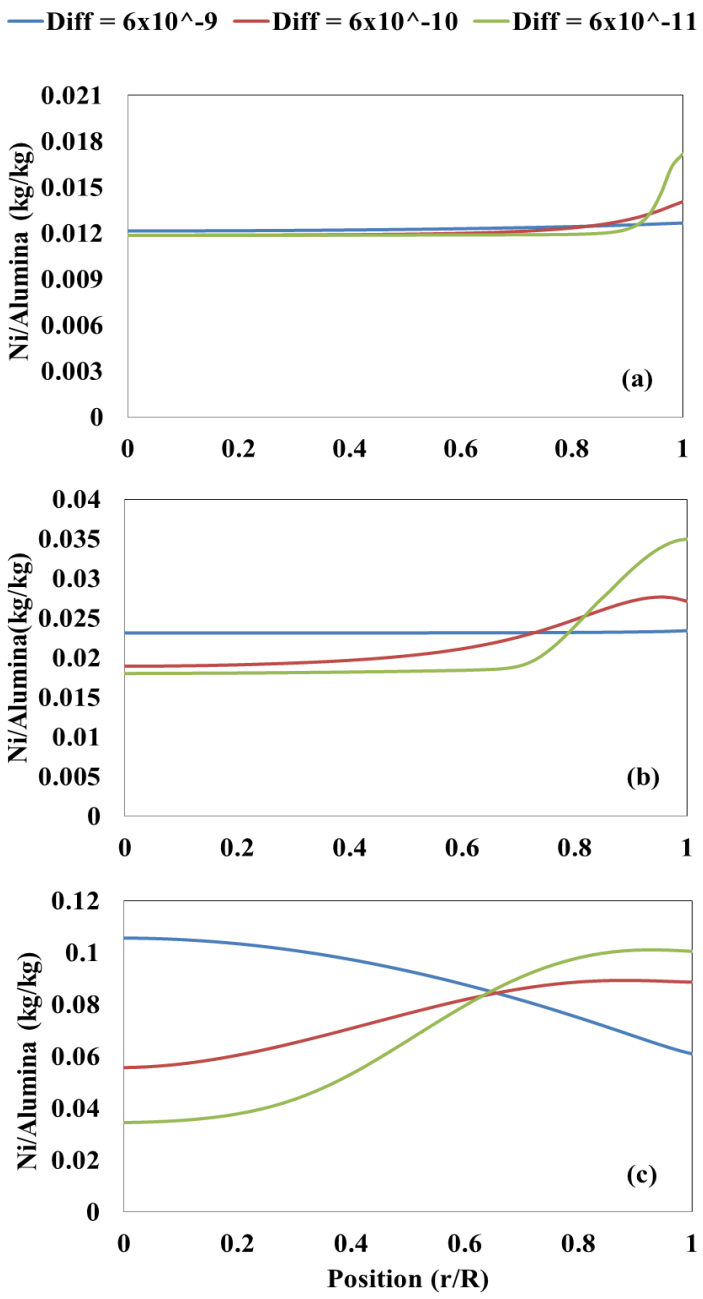

Figure 19: Reduced parameter model simulation results comparing post drying metal distributions for different diffusion co-efficient values of nickel nitrate hexahydrate over γ-Alumina. Results show distribution from center of the support to surface of the support, dried at 80^0C and a uniform initial condition for different metal loadings (a) 0.01 M, (b) 0.1 M and (c) 1.0 M

3.3.3 Summary

The analysis of the high concentration model with solution properties and adsorption parameters gives us a simplified model - the reduced parameter model. This model can now be applied to drying of any metal precursor on γ-alumina supports without having to repeat expensive and time consuming experiments. The parameters that play a key role in the metal distribution are the volume ratio of metal, the vapor pressure, the kinetic equilibrium constant, the saturation concentration and the diffusion co-efficient. Out of these five parameters, the saturation concentration and kinetic equilibrium values are obtained from a single experiment and another experiment will have to be performed to determine the volume ratio of metal. The diffusion co-efficient is obtained from literature and the vapor pressure is obtained from Raoult's law which is calculated based on the concentration of the metal solution.

The PARSIM Fortran code which includes the original and reduced parameter version in an extremely complex code with multiple files enclosed. If you would like a copy of the code please contact Dr. Benjamin J. Glasser (bglasser@scarletmail.rutgers.edu).

3.3.4 New metal predictions

To test the functionality and precision of our reduced parameter model, we chose a new metal – cobalt nitrate hexahydrate. Cobalt catalyst research is an area of importance to chemical process industry due to their extensive application in a range of industrial processes. Their applications are commonly found in the fields of catalysis, solid-state gas sensors, magnetic

materials, electro-chromic devices, and high-temperature solar collectors[47]. As a catalyst, cobalt is mainly used in the Fischer−Tropsch synthesis [48, 49]. Cobalt nitrate hexahydrate is used for our experiment here, which is a crystalline red-brown solid (Sigma-Aldrich, St. Louis, MO, USA). γ-alumina cylindrical pellets from provided by Saint-Gobain Norpro were used as supports (section 2.2).

We then performed two experiments described in section 2.2.1 and 2.2.4 and in fig. 2 and fig. 6 to determine the volume ratio of metal, kinetic equilibrium constant (K_{eq}) and saturation concentration (C_{sat}) respectively for cobalt nitrate hexahydrate. Again, a UV-Visible spectrometer was used to determine the concentration of cobalt nitrate in solution with peaks observed at 500nm.

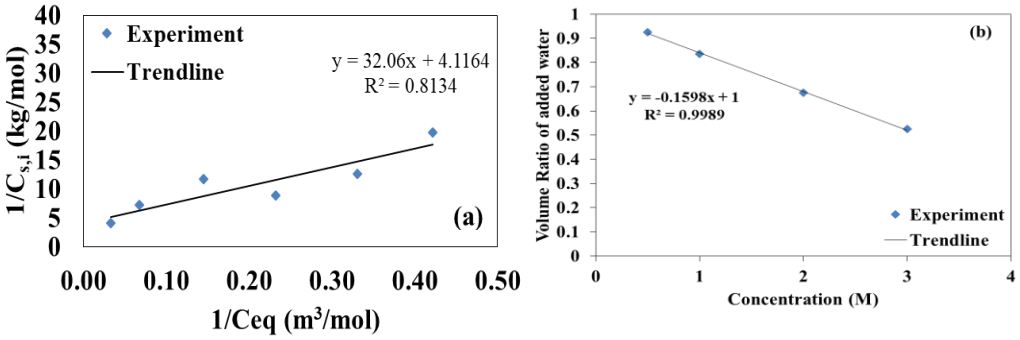

Figure 20: (a) Plot showing the effect of adsorption concentration on the equilibrium concentration for different concentrations of Cobalt nitrate hexahydrate on γ-Alumina supports at room temperature (25^0C). (b) Plot showing volume ratio of metal for different concentrations cobalt nitrate hexahydrate at room temperature.

The volume ratio of metal was obtained as 0.159* concentration of cobalt nitrate. The kinetic equilibrium constant and saturation concentration were

obtained as 0.12 m^3/mol and 0.2 mol/kg respectively (see Fig. 20). These values were then incorporated into our reduced parameter model along with the diffusion coefficient value obtained from literature (0.732 x 10^{-10} m^2/s) [50]. Predictions were generated for post drying metal distribution of cobalt nitrate over γ- alumina and were compared to experimental metal profiles. Different concentrations of cobalt nitrate were studied (not shown here). The drying temperature was kept at 80^0C and the drying process mentioned in section 2.2 and section 3.1 were followed. Experimental metal profiles for two concentrations (0.1 M and 0.5 M) from three different supports for each case were compared to the profiles generated from this model (see fig. 21). This allows us to observe the differences from support to support. The reduced parameter model shows an appreciable agreement with the experimental profiles for both 0.1 M and 0.5 M.

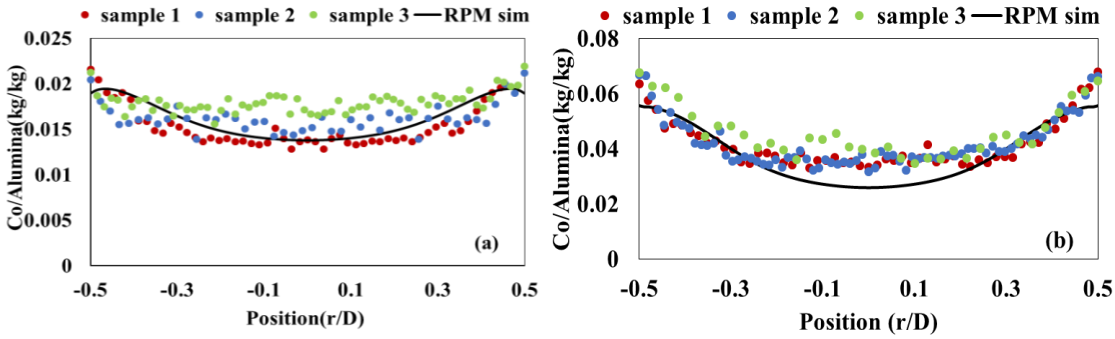

Figure 21: Reduced parameter model simulation results comparing post drying metal distributions for cobalt nitrate hexahydrate over γ-alumina to experimental profiles. Results show distributions from surface to surface of the support, dried at 80^0C and a uniform initial condition for two different metal loadings (a) 0.1 M and (b) 0.5 M

4. Conclusion

Through this research, we created a new model - the reduced parameter model, which is an abridged model derived from principles of the high concentration model. This model can be used to predict metal distributions and drying behavior with different metal precursors on the same given support specifications (γ-alumina). The model is based on simulation results derived from the high concentration model using a nickel nitrate hexahydrate/alumina system at different metal loadings and 80^0C drying temperature. Adsorption and transport parameters are derived from separate experiments/calculations. In the due course of this parametric analysis, several interesting phenomena were observed:

The volume ratio of metal has a noticeable effect on the metal distribution after drying. This is prominent at higher concentrations. Hence, this parameter would vary from metal to metal and have a pronounced effect of the metal distribution. The vapor pressure from Raoult's law is calculated based on the concentration of metal precursor in solution and it is also seen that there is a great reduction in vapor pressure at high concentrations. We could achieve a close match to the existing high concentration model by the inclusion of just these two solution based parameters.

The adsorption effects were more prominent on metal distributions at lower concentrations. The adsorption is driven by equilibrium attainment at lower concentrations and by saturation concentration at higher concentrations.

However, the kinetic adsorption constant is not an essential parameter affecting metal distributions. This could be due to the uniform initial condition, which assumes that drying begins after equilibrium is attained. However, for a non-uniform condition, differences maybe be observed.

Hence, for a new metal precursor, three parameters would have to be determined from experiments: the volume ratio of metal, the kinetic equilibrium constant and the saturation concentration of metal on support. These three crucial properties can be obtained through two simple experiments in total and then can be incorporated into the model. The diffusion coefficient is obtained from literature and added into the model. With all the other values left unchanged we will be able to obtain predictions for new metals equivalent to those from the high concentration model.

The simulation predictions for different loadings of cobalt nitrate help us understand how the model would function on metals other than nickel nitrate hexahydrate. However many more concentration cases are to be studied and validated for this model. In the case of 0.5 M (see Fig. 19), a better agreement with experimental profiles could be achieved. Future work could include working on other concentration cases and different drying temperatures to improve the robustness of this model.

On the brighter side, the reduced parameter model is an efficient tool that would allow us to generate predictions for different metal precursors used in the industry. The predictions would save a lot of time spent on experiments

and would also optimize metal precursor expenses, especially in case of expensive metals like palladium.

Reference

[1] F. Pinna, "Supported metal catalysts preparation," *Catalysis Today,* vol. 41, pp. 129-137, 1998.

[2] P. E. d. J. Peter Munnik, and Krijn P. de Jong, "Recent Developments in the Synthesis of Supported Catalysts " *Chemical Review,* p. 6687−6718, 06/09/2015 2015.

[3] A. J. Louise Samain, Mattias Edén, Danielle M. Ladd, Dong-Kyun Seo, F. Javier Garcia-Garcia, Ulrich Häussermann "Structural analysis of highly porous γ-Al2O3," *Journal of Solid State Chemistry,* vol. 217, pp. 1-8, 2014.

[4] H. W. Richardson, *Handbook of Copper Compounds and Applications*. Taylor & Francis, 1997.

[5] X. Liu, J. G. Khinast, and B. J. Glasser, "Drying of Supported Catalysts: A Comparison of Model Predictions and Experimental Measurements of Metal Profiles," *Industrial & Engineering Chemistry Research,* vol. 49, no. 6, pp. 2649-2657, 2010/03/17 2010.

[6] A. L. G. Karaiskakis, N. A, Katsanos, "Kinetic Study of the Drying Step of Supported Catalysts by Reversed-Flow Gas Chromatography," *Chromatographia* vol. 15, no. 6, pp. 351-354, 1982.

[7] D. M. Parikh. (2014). *SOLIDS DRYING: BASICS AND APPLICATIONS*.

[8] E. W. Jerger, "Mechanism of moisture movement in the drying of organic granular solids," 1951.

[9] A. S. A. Al-Fatesh and A. H. Fakeeha, "Effects of calcination and activation temperature on dry reforming catalysts," *Journal of Saudi Chemical Society,* vol. 16, no. 1, pp. 55-61, 2012/01/01/ 2012.

[10] M. Komiyama, R. P. Merrill, and H. F. Harnsberger, "Concentration profiles in impregnation of porous catalysts: Nickel on alumina," *Journal of Catalysis,* vol. 63, no. 1, pp. 35-52, 1980/05/01/ 1980.

[11] S.-Y. Lee and R. Aris, "The Distribution of Active ingredients in Supported Catalysts Prepared by Impregnation," *Catalysis Reviews,* vol. 27, no. 2, pp. 207-340, 1985/06/01 1985.

[12] N. Santhanam, T. A. Conforti, W. Spieker, and J. R. Regalbuto, "Nature of metal catalyst precursors adsorbed onto oxide supports," *Catalysis Today,* vol. 21, no. 1, pp. 141-156, 1994/08/30/ 1994.

[13] G. H. Van Den Berg and H. T. Rijnten, "The Impregnation and Drying Step in Catalyst Manufacturing," in *Studies in Surface Science and Catalysis*, vol. 3, B. Delmon, P. Grange, P. Jacobs, and G. Poncelet, Eds.: Elsevier, 1979, pp. 265-277.

[14] A. V. Neimark, L. I. Kheifets, and V. B. Fenelonov, "Theory of preparation of supported catalysts," *Industrial & Engineering Chemistry Product Research and Development,* vol. 20, no. 3, pp. 439-450, 1981/09/01 1981.

[15] C. Hao, "Belt drying of supported catalysts," (in eng), 2015.

[16] W. D. Li, Y. W. Li, Z. F. Qin, and S. Y. Chen, "Theoretical prediction and experimental validation of the egg-shell distribution of Ni for supported ni/Al20O3 catalysts," *Chemical Engineering Science,* vol. 49, no. 24, Part A, pp. 4889-4895, 1994/01/01/ 1994.

[17] M. Börnhorst *et al.*, "Influence of pore structure and impregnation–drying conditions on the solid distribution in porous support materials," *Drying Technology,* vol. 34, no. 16, pp. 1964-1978, 2016/12/09 2016.

[18] J. Mahadevan, M. M. Sharma, and Y. C. Yortsos, "Flow- through drying of porous media," *AIChE Journal,* vol. 52, no. 7, pp. 2367-2380, 2006.

[19] A. Lekhal, B. J. Glasser, and J. G. Khinast, "Impact of drying on the catalyst profile in supported impregnation catalysts," *Chemical Engineering Science,* vol. 56, no. 15, pp. 4473-4487, 2001/08/01/ 2001.

[20] A. Lekhal, B. J. Glasser, and J. G. Khinast, "Influence of pH and ionic strength on the metal profile of impregnation catalysts," *Chemical Engineering Science,* vol. 59, no. 5, pp. 1063-1077, 2004/03/01/ 2004.

[21] A. Lekhal, J. G. Khinast, and B. J. Glasser, "Predicting the Effect of Drying on Supported Coimpregnation Catalysts," *Industrial & Engineering Chemistry Research,* vol. 40, no. 18, pp. 3989-3999, 2001/09/01 2001.

[22] X. Liu, J. G. Khinast, and B. J. Glasser, "A parametric investigation of impregnation and drying of supported catalysts," *Chemical Engineering Science,* vol. 63, no. 18, pp. 4517-4530, 2008/09/01/ 2008.

[23] X. Liu, J. G. Khinast, and B. J. Glasser, "Drying of Ni/Alumina Catalysts: Control of the Metal Distribution Using Surfactants and the Melt Infiltration Method," *Industrial & Engineering Chemistry Research,* vol. 53, no. 14, pp. 5792-5800, 2014/04/09 2014.

[24] X. Liu, J. G. Khinast, and B. J. Glasser, "Drying of supported catalysts for low melting point precursors: Impact of metal loading and drying methods on the metal distribution," *Chemical Engineering Science,* vol. 79, no. Supplement C, pp. 187-199, 2012/09/10/ 2012.

[25] M. Morbidelli, A. Gavriilidis, and A. Varma, *Catalyst Design: Optimal Distribution of Catalyst in Pellets, Reactors, and Membranes*. Cambridge University Press, 2005.

[26] A. J. van Dillen, R. J. A. M. Terörde, D. J. Lensveld, J. W. Geus, and K. P. de Jong, "Synthesis of supported catalysts by impregnation and drying using aqueous chelated metal complexes," *Journal of Catalysis,* vol. 216, no. 1, pp. 257-264, 2003/05/01/ 2003.

[27] F. J. Cherne, III and P. A. Deymier, "Calculation of viscosity of liquid nickel by molecular dynamics methods," (in English), 1998-11-03 1998.

[28] J. B. Irving and N. E. Laboratory, *Viscosities of Binary Liquid Mixtures: The Effectiveness of Mixture Equations*. National Engineering Laboratory, 1977.

[29] W. D. Monnery, W. Y. Svrcek, and A. K. Mehrotra, "Viscosity: A critical review of practical predictive and correlative methods," *The Canadian Journal of Chemical Engineering,* vol. 73, no. 1, pp. 3-40, 1995.

[30] S. K. Jain, "Density, viscosity, and surface tension of mixed molten hydrates. 2. Mixtures of zinc nitrate and nickel nitrate hexahydrates," *Journal of Chemical & Engineering Data,* vol. 25, no. 1, pp. 36-40, 1980/01/01 1980.

[31] N. D. Azizov and A. B. Zeinalova, "The Density and Partial Molar Volume of Aqueous Solutions of Nickel Nitrate at High Parameters of State," *High Temperature,* journal article vol. 42, no. 4, pp. 648-651, July 01 2004.

[32] M. Laliberté, "Model for Calculating the Viscosity of Aqueous Solutions," *Journal of Chemical & Engineering Data,* vol. 52, no. 2, pp. 321-335, 2007/03/01 2007.

[33] M. Laliberté, "A Model for Calculating the Heat Capacity of Aqueous Solutions, with Updated Density and Viscosity Data," *Journal of Chemical & Engineering Data,* vol. 54, no. 6, pp. 1725-1760, 2009/06/11 2009.

[34] M. Laliberté and W. E. Cooper, "Model for Calculating the Density of Aqueous Electrolyte Solutions," *Journal of Chemical & Engineering Data,* vol. 49, no. 5, pp. 1141-1151, 2004/09/01 2004.

[35] H. W. Kim, K. M. Kang, and H.-Y. Kwak, "Preparation of supported Ni catalysts with a core/shell structure and their catalytic tests of partial oxidation of methane," *International Journal of Hydrogen Energy,* vol. 34, no. 8, pp. 3351-3359, 2009/05/01/ 2009.

[36] Y.-X. Pan, C.-J. Liu, and P. Shi, "Preparation and characterization of coke resistant Ni/SiO2 catalyst for carbon dioxide reforming of methane," *Journal of Power Sources,* vol. 176, no. 1, pp. 46-53, 2008/01/21/ 2008.

[37] H. R. Reinhoudt, R. Troost, A. D. van Langeveld, J. A. R. van Veen, S. T. Sie, and J. A. Moulijn, "The Nature of the Active Phase in Sulfided NiW/γ-Al2O3 in Relation to Its Catalytic Performance in Hydrodesulfurization Reactions," *Journal of Catalysis,* vol. 203, no. 2, pp. 509-515, 2001/10/25/ 2001.

[38] D. C. R. M. Santos, J. S. Lisboa, F. B. Passos, and F. B. Noronha, "Characterization of steam-reforming catalysts," *Brazilian Journal of Chemical Engineering,* vol. 21, pp. 203-209, 2004.

[39] F. Melo, J. Cervelló, and E. Hermana, "Impregnation of porous supports—I theoretical study of the impregnation of one or two active species," *Chemical Engineering Science,* vol. 35, no. 10, pp. 2165-2174, 1980/01/01/ 1980.

[40] P. Papageorgiou, D. M. Price, A. Gavriilidis, and A. Varma, "Preparation of Pt/γ-Al2O3Pellets with Internal Step-Distribution of Catalyst: Experiments and Theory," *Journal of Catalysis,* vol. 158, no. 2, pp. 439-451, 1996/02/01/ 1996.

[41] O. A. Sceiza, Castro,A.A.,Ardlles,D.R.,Parera,J.M.,, "Modeling of the impregnation step to prepare supported Pt/Al2O3 catalysts," *Industrial & Engineering Chemistry Research (ACS Publications),* vol. 25, pp. 84-88, 1986.

[42] R. Krishna, "A simplified procedure for the solution of the dusty gas model equations for steady-state transport in non-reacting systems," *The Chemical Engineering Journal,* vol. 35, no. 2, pp. 75-81, 1987/06/01/ 1987.

[43] E. Bender, "Numerical heat transfer and fluid flow. Von S. V. Patankar. Hemisphere Publishing Corporation, Washington – New York – London. McGraw Hill Book Company, New York 1980. 1. Aufl., 197 S., 76 Abb., geb., DM 71,90," *Chemie Ingenieur Technik,* vol. 53, no. 3, pp. 225-225, 1981.

[44] P. Deuflhard, E. Hairer, and J. Zugck, "One-step and extrapolation methods for differential-algebraic systems," *Numerische Mathematik,* journal article vol. 51, no. 5, pp. 501-516, September 01 1987.

[45] F. K. Hansen and G. Rødsrud, "Surface tension by pendant drop: I. A fast standard instrument using computer image analysis," *Journal of Colloid and Interface Science,* vol. 141, no. 1, pp. 1-9, 1991/01/01/ 1991.

[46] R. Takahashi, S. Sato, T. Sodesawa, and H. Nishida, "Effect of pore size on the liquid-phase pore diffusion of nickel nitrate," *Physical Chemistry Chemical Physics,* 10.1039/B202024F vol. 4, no. 15, pp. 3800-3805, 2002.

[47] M. H. LIM, T. H. PARK, J. H. GU, and Y. YU, "Cobalt oxide catalysts," ed: Google Patents, 2007.

[48] N. Fischer, E. van Steen, and M. Claeys, "Structure sensitivity of the Fischer–Tropsch activity and selectivity on alumina supported cobalt catalysts," *Journal of Catalysis,* vol. 299, pp. 67-80, 2013/03/01/ 2013.

[49] L. A. Richard, P. Moreau, S. Rugmini, and F. Daly, "Fischer-Tropsch performance correlated to catalyst structure: Trends in activity and stability for a silica-supported cobalt catalyst," *Applied Catalysis A: General,* vol. 464-465, pp. 200-206, 2013/08/15/ 2013.

[50] J. Buffle, Z. Zhang, and K. Startchev, "Metal Flux and Dynamic Speciation at (Bio)interfaces. Part I: Critical Evaluation and Compilation of Physicochemical Parameters for Complexes with Simple Ligands and Fulvic/Humic Substances," *Environmental Science & Technology,* vol. 41, no. 22, pp. 7609-7620, 2007/11/01 2007.